NASA/TM—98-201792

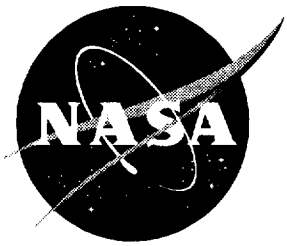

Capture of Hypervelocity Particles With Low-Density Aerogel

Friedrich Hörz, Mark J. Cintala, and Michael E. Zolensky
NASA Johnson Space Center

Ronald B. Bernhard, William E. Davidson, Gerald Haynes, and Thomas H. See
Lockheed-Martin Space Mission Systems and Services

Peter Tsou
Jet Propulsion Laboratory

Donald E. Brownlee
University of Washington

National Aeronautics and
Space Administration

Lyndon B. Johnson Space Center
Houston, Texas

April 1998

Available from:

NASA Center for AeroSpace Information
800 Elkridge Landing Road
Linthicum Heights, MD 21090-2934
Price Code: A17

National Technical Information Service
5285 Port Royal Road
Springfield, VA 22161
Price Code: A10

Contents

Figures

Contents

(continued)

Figures (continued)

Summary

Impact experiments into low-density (0.01-0.05 g/cm^3) SiO_2 aerogel targets have been conducted using a variety of spherical projectiles, including 2024 aluminum, aluminum oxide, and soda-lime glass, irregular particles of the Allende and Pampa-A meteorites obtained by crushing, and single-crystal fragments of olivine and pyrrhotite. All projectiles were between 43 and 54 μm in diameter, and impact velocities ranged from 3 to 7 km/s. Our objective was to evaluate the performance of low-density aerogels for inclusion in space-borne flight instruments whose aim is to capture natural and man-made hypervelocity particles in the least destructive fashion, hopefully without melting. Such capture media were recently exposed on space station *Mir* and are under development for *Stardust*, a Discovery-class mission. These captured-particle residues will be returned to Earth for detailed mineralogic, chemical and isotopic analyses to characterize their respective source areas and formative processes. Previous studies demonstrated the basic utility of aerogel in accomplishing these capture objectives. In an attempt to simulate actual flight-conditions with improved fidelity, the current experiments employ lower-density aerogels, as well as smaller projectiles than most previous work.

Our experiments show that definition of the initial impact conditions for such small impactors (<100 μm diameter) poses a substantial experimental challenge when using light-gas guns and associated shot-gunning methods for particle acceleration. Individual projectiles, including precision microspheres of glass and aluminum, will inherently vary in size and mass proportionate with the mesh-openings of the sieves employed. In addition, all projectiles manufactured by the crushing of coarser materials, whether man-made or natural, will contain microcracks and other flaws that cause individual particles to fragment during launch, thereby inhibiting any control of the exact projectile size, mass, and shape. As a result of these experimental limitations, past and present experiments are characterized by poor reproducibility and large data scatter. Consequently, there is currently no reliable experimental basis to utilize penetration tracks in aerogels for the reconstruction of the initial mass or encounter velocity of man-made orbital debris or natural cosmic-dust particles as already noted and emphasized by Burchell and Thomson (1996). Improved control of the initial size, mass, and shape of the projectile(s) is needed to yield more reproducible experiments and a more reliable basis to understand the deceleration of very small hypervelocity impactors by targets of very low density and exceptionally high porosity.

Nevertheless, we found that the density of aerogel affects the length of the resulting penetration track. For soda-lime glass spheres of 50 μm diameter at 6 km/s, the track length (l) normalized to projectile diameter (Dp) is l/Dp = 60-80, 120-150, and 400-450 using aerogels of 0.1, 0.05 and 0.01 g/cm^3 density, respectively. The relationship of track length to impact velocity is complex, as was previously observed for porous Al_2O_3 (Werle et al., 1981) and Styrofoam (Tsou, 1990) targets. Our experiments showed that 50-μm glass spheres penetrate deeper at 5 km/s than at 6 km/s. In addition, we conducted experiments at oblique impact angles (30°, 45°, and 60° from normal incidence) while holding the density of the aerogel constant (0.02g/cm^3) and varying the impact velocity from 3 to 6 km/s. The resulting penetration tracks faithfully recorded the angle of incidence relative to the collector surface, as earlier reported by Thomson (1995), yet the absolute track length was unaffected by impact angle. This behavior is unlike that found with projectile penetration into higher-density targets, where the absolute crater depth depends strongly on the impact angle. These observations lend strong support for the model of Anderson and Ahrens (1994), which suggests that most deceleration of hypervelocity particles in highly porous, low-density targets is governed by viscous drag rather than by classical shock and cratering processes.

In addition, we simulated the impact of "fluffy" natural particles, presumably very friable and porous, for which there is some concern about their efficiency of capture. Two approaches were used. One employed compressed cocoa powder, which was loaded into the sabot cavity, that did not disperse sufficiently during free flight resulting in small clumps (on the scale of 100 μm) impacting the aerogel target. These clumps produced characteristic short and stubby tracks that were lined with remnants of cocoa powder. The second approach employed a 4-μm-thick aluminum bumper foil that was easily penetrated by 50-μm glass spheres, yet was sufficiently thick to disrupt each projectile, thus generating a cloud of projectile fragments that could be intercepted with the aerogel target downrange. These aerogel targets were located at variable standoff distances (L) from the bumper foil such that either tightly clustered or widely dispersed fragment clouds would impinge on the aerogel. The resulting impact features faithfully record the detailed mass distribution of these fragment clouds, as evidenced by tightly clustered or (arbitrarily) dispersed penetration tracks of widely variable depth. Projectile residues were found at the termini of many of these subsidiary tracks.

These experiments show aerogel's efficiency in capturing analyzable residue of hypervelocity projectiles, including fluffy particles at impact velocities of ~6 km/s, the applicable encounter velocity for the *Stardust* spacecraft with Comet Wild 2. In addition, differentiation between metallic and oxidized aluminum-rich impactors in low Earth orbit, the major objective of the orbital debris collector on *Mir*, should be readily accomplished at the somewhat higher mean encounter velocities (9-10 km/s) that are typical for man-made debris in low Earth orbit. Finally, the direction of impact relative to the collector surface can be deduced from the inclination of individual penetration tracks. However, current empirical or theoretical understanding of aerogel penetration processes is insufficient to reconstruct projectile mass and impact velocity from the measured dimensions of penetration tracks and/or the mass of the residue. If required by scientific need, other concepts are available to independently determine projectile mass and detailed trajectory elements on a particle by particle basis in free flight, prior to impact and capture by aerogel (e.g., Auer and Bun, 1994).

1. Introduction

This report summarizes laboratory impact experiments aimed at evaluating the suitability of SiO_2 aerogel for the collection of hypervelocity particles on space-exposed flight instruments. As recently summarized by Tsou (1995), such aerogels constitute a unique class of low-density, highly porous materials (Fricke, 1988; Hrubesh and Poco, 1990) that are capable of decelerating high-velocity particles without substantial melting, or other modifications of their component materials. This is in stark contrast to high-velocity impact into dense targets that result in complete melting, if not vaporization, of the impactor during the formation of a hypervelocity impact crater. Consequently, such aerogels appear to be suitable for the capture of natural cosmic-dust particles and/or man-made debris in such a manner that their residues may be returned to Earth for a wide variety of detailed mineralogic, chemical, and isotopic analyses. Thus, aerogel capture is a promising approach for detailed investigation of the natural and man-made particle environment in space, and the asteroidal, cometary, or man-made sources of those particles (e.g., Tsou et al., 1988; CDCF, 1990; Zolensky, 1994; Brownlee et al., 1994).

Specifically, this report summarizes recent experiments conducted in the Experimental Impact Laboratory at the Johnson Space Center (JSC) in support of two flight instruments. One of these instruments, the orbital debris collector (ODC), was recently returned following an ~18-month exposure on the space station *Mir*, while the other will be on board the *Stardust* spacecraft, a Discovery-class mission to comet Wild 2 (*Stardust* experiment).

ODC's primary purpose was to evaluate the man-made particle environment in *Mir*'s high-inclination orbit (51°) for comparison with instruments exposed by the Shuttle and the Long-Duration Exposure Facility (LDEF), both of which represent modest inclination orbits (28°). LDEF revealed numerous types of natural and man-made particles, including a common subgroup that is composed entirely of aluminum (Al), either metallic or oxidized, and that must derive from man-made sources in highly elliptical orbits (Bernhard et al., 1996). While ODC indiscriminately trapped all types of particles in low Earth orbit (LEO), its major objective is to assess the relative frequency of Al particles, and specifically, the relative roles of metallic versus oxidized species. ODC was deployed on the *Mir* complex on March 23, 1996, and was retrieved in October 1997. It exposed an array of 72 individual SiO_2 aerogel samples, each 10 x 10 cm in surface area and ~12 mm thick, all of 0.02 g/cm^3 bulk density.

The *Stardust* spacecraft is currently scheduled for launch in 1999 and will fly through the coma of Comet Wild 2 in 2003 at a distance of about 100 km and a velocity of approximately 6 km/s relative to the comet nucleus. This is an extraordinarily low-encounter velocity, well within laboratory impact-simulation capabilities, and in a velocity regime for which the successful recovery of unmolten projectile residue has been demonstrated by a number of experimental studies (e.g., Tsou et al., 1988; Barrett et al., 1992; Mendez, 1995). After comet passage, the *Stardust* spacecraft will return to Earth orbit in 2007. The aerogel collectors will be housed inside an atmospheric reentry capsule that will be parachuted for recovery on land. Commensurate with its significance as the first extraterrestrial sample-return mission since Apollo, optimization of the *Stardust* aerogel collector medium constitutes a high-priority development effort, both experimental and theoretical. In situ measurements and observations of comet Halley dust by the Giotto Spacecraft (Kissel

et al., 1986; Grewing et al., 1986; Jessberger et al., 1989) suggest that a wide range of particle sizes may be encountered, as well as a range of particle compositions and physical properties.

The basic objectives for the development of suitable aerogel-collector materials for the *Mir* and *Stardust* instruments relate to a detailed understanding of the deceleration process and the associated thermal environment that controls the yield of unmelted residue mass. How will these deceleration processes affect the mineralogic, chemical, and isotopic characteristics of the initial impactors and how much mass will be lost in the process? Recovery of hypervelocity projectiles varying widely in size, mass, and chemical and physical properties is a prerequisite for any successful particle collector. Consequently, the potentially nondestructive deceleration of highly diverse natural and man-made particles in space by (ideally) a single target medium constitutes a most challenging development task.

This report summarizes a variety of pilot-type impact experiments recently conducted at JSC to arrive at a general overview of the performance of SiO_2 aerogel (Hrubesh and Poco, 1990), or simply "aerogel" throughout this report for the sake of brevity. The objective was to identify and define first-order issues for additional development, if needed. As a consequence, a variety of topics were addressed that had been recognized as potentially important in previous aerogel studies, or on the basis of general cratering studies in dense-target media. Clearly, some of the present work was guided by earlier studies using aerogel targets (e.g., Tsou et al., 1988, 1995; Barrett et al., 1992; Mendez, 1995; Thomson, 1995; Burchell and Thomson, 1996). In addition, non-SiO_2, low-density, highly porous materials have been used previously, and have provided important general insights into the capture performance of low-density target media such as porous Al_2O_3 (Werle et al., 1981), Styrofoam (Tsou, 1990), and other foamed polymers (Maag et al., 1992). Cumulatively, these experiments demonstrated that the recovery of unmolten projectiles and/or fragments is feasible in highly porous materials at velocities as high as 7 km/s. Given the relatively small number of past experiments, combined with a wide range of projectile sizes, materials, and target-media and associated densities, it is difficult to synthesize the existing work into a systematic database that could guide, with confidence, the design and interpretation of the *Mir* and/or *Stardust* flight collectors; a similar conclusion was reached by Tsou (1995), and Burchell and Thomson (1996).

The present experiments were conceived to complement these previous efforts by employing smaller projectiles, typically 50 μm in diameter, than previous studies (typically >100 μm, if not >1000 μm). Experimentation with such small projectiles is desirable for the realistic, dimensional scaling of projectile size and physical target structure. Aerogels are composed of irregular chains and clusters of SiO_4-tetrahedra that are typically 4-6 nm thick and 20-30 nm long (e.g., Fricke, 1988). The smaller the particle to be captured, the larger the relative size of these SiO_4 clusters and the more pronounced potential shock effects and associated heating of the projectile. Therefore, it is important to evaluate the utility of aerogel with projectiles that approach or duplicate the size(s) of particles in space. We also employed aerogels of lower density, 0.01 to 0.05 g/cm^3, compared to most of the previous work at >0.05 g/cm^3; materials <0.05 g/cm^3 are now readily available, yet were somewhat experimental and of low transparency in the past (see also Tsou, 1995). Furthermore, we experimented over a wider range in velocity (3-7 km/s) than most of the previous studies, and we investigated the effects of oblique impact. Some experiments simulated for the first time the impact of

projectiles of low-cohesive strength. The overall objective was to conduct experiments with a high degree of fidelity relative to space-exposed aerogel collectors, and to vary some initial impact parameters (e.g., velocity and aerogel density) in a more systematic fashion than was the case in most of the earlier studies. The expected result was an improved empirical and theoretical understanding of the deceleration process in aerogel and of associated effects regarding possible particle modification(s).

The most comprehensive set of experiments with low-density targets that is available employed Al projectiles and Styrofoam targets (Tsou, 1990). These data were utilized by Anderson and Ahrens (1994) to arrive at a first-order model of deceleration processes in highly foamed, low-density media, which describes the capture of hypervelocity particles in such materials as the result of shock processes and those governed by classical continuum mechanics, including viscous drag and ablation. While the Anderson and Ahrens (1994) model is not readily transferred to SiO_2 without additional model assumptions, it is obvious that projectile size as well as bulk target density and internal structure will play crucial roles. It is for these reasons that we experimented with very small impactors and employed aerogels of variable density, duplicating those exposed on *Mir* and contemplated for *Stardust*.

Unfortunately, the experiments described below must be considered somewhat qualitative because they are afflicted with some experimental uncertainties, as detailed throughout this report. Most of our experimental data are characterized by substantial, if not intolerable, scatter, akin to that emphasized recently in the most systematic aerogel studies to date by Thomson (1995) and Burchell and Thomson (1996). Evidence suggests that this scatter is largely due to experimental difficulties in duplicating given sets of initial impact conditions, notably constant size, mass, or shape of very small, individual projectiles. Such projectiles can only be launched as an ensemble of particles in light-gas guns, and therefore can be characterized only by a range of (sieved) sizes without good control of mass or shape on a particle-by-particle basis. To complicate matters, many projectile materials tend to break apart during light-gas gun acceleration, producing a wide spectrum of impactor sizes and masses. In addition, reproducibility of exact aerogel density may be difficult to accomplish. As a result, variations in target density may be a contributing factor in producing large variances from experiment to experiment. Having recognized some of these experimental difficulties, we hope to eliminate some of them in the near future to improve on the reproducibility of individual experiments.

This document represents an informal progress report. Emphasis is on photographic documentation and some first-order dimensional analysis of penetration tracks and projectile residues. As stated above, a wide variety of independent topics will be addressed in this report. Some might be woefully incomplete in the reader's view, yet they are consistent with pilot-type experimentation and associated evaluations. The report is in approximate, chronological sequence, as we wish to guide the reader through some of the experimental difficulties in approximately the time-sequence in which they were encountered and recognized. Also note that the existence of projectile residue at the end of individual penetration tracks was only determined, in many cases, via binocular microscope. Few residues were physically recovered, and even fewer were analyzed in detail using scanning electron microscope (SEM) and associated energy dispersive X-ray spectroscopy (EDS) or transmission electron microscope methods; such detailed analyses were not within the scope or resources of the current effort.

2. Experimental Objectives

The experiments conducted to date fall into two categories along the following major objectives:

(1) Qualitatively demonstrate that the collection of unmolten projectile residues of silicates is feasible at impact velocities applicable to *Stardust* (~6.1 km/s), and explore the effects of aerogel density on the efficiency of capture and the degradation of initial particle properties. In addition, determine how well particles can be captured that are of relatively low cohesion and high porosity, and which are thought to be relatively abundant among cometary dust grains. Establish the survivability of metallic- and oxidized-aluminum impactors in aerogel at impact velocities of 7 km/s in support of ODC, and compare the residues of brittle silicates, ductile metal, and highly refractory oxide impactors. In short, this objective related to the empirical recovery and mineralogic-petrographic characterization of analyzable residues of a diversity of projectiles.

(2) Collect a suitable experimental database—over a wide range of aerogel density, impact velocity, and projectile materials—for the development of theoretical models and a more general understanding of the physical processes that govern particle deceleration and associated heating in aerogel targets. These highly parametric tests may be qualified as "calibration" experiments as they relate the initial impact conditions to the dimensional characterization of the resulting impact features and associated projectile residues.

Most experiments documented in this report relate to both objectives, which is why implications for the capture and calibration objectives are not separated rigorously throughout this report. In this report, Sections 1 and 2 provide background, while Section 3 details experimental procedures, including target preparation and projectile selection. Sections 4 through 6 describe the experimental results. Section 4 addresses the length of penetration tracks at normal projectile incidence and as a function of aerogel density, impact velocity, and projectile materials; it also introduces some of the limitations of launching a collection of small particles with light-gas guns. Section 5 details the length of penetration tracks as a function of impact angle and velocity at otherwise constant impact conditions, while Section 6 describes impacts by projectiles of low-density/low-cohesive strength. Section 7 provides a general discussion of current and past results.

3. Experimental Procedures and Limitations

3.1 Light-Gas Gun Operations

Impact experiments were carried out with a small-caliber (5 mm), light-gas gun that was used as a high-velocity, small-scale version of a shotgun. Ensembles of 50-100 projectiles (50 μm in diameter) were accelerated via a four-piece, serrated sabot. Before launch, the projectiles reside in a 0.5-mm-diameter, 2- to 3-mm-long cylindrical cavity at the front of the 5-mm-diameter, 4- to 6-mm-long sabot. Upon exiting the muzzle, the petals of the sabot and most of the projectiles radially separate, being stopped by collision with a massive steel aperture about 5 m downrange. A concentric hole in the aperture permits only the central cluster of projectiles to proceed downrange to impact the target, which is about 4 m further downrange from the aperture. This latter flight section contains additional mechanical apertures, such that a relatively small number of projectiles—typically 2-5 and occasionally as many as 10—encounter the target which, in this case, was

monolithic aerogel squares of variable thickness measuring roughly 5 cm x 5 cm. The majority of hydrogen driver-gas used to accelerate the sabot is blocked with a mechanical flapper valve. Carbon-rich vapors and particulates from a variety of sources, including the sabot, high-pressure diaphragm, pump-tube piston, and launch-tube abrasion, are largely trapped by additional mechanical apertures. As a result, the delicate aerogel surfaces remain undisturbed and sufficiently clean to permit direct transfer to an SEM for imaging purposes and associated chemical analysis by EDS.

The front face of the aerogel target is monitored by a photodiode that records the light flashes of individual projectile impacts (at times t_1, t_2, t_3,... t_n) via digital-storage oscilloscopes (Tektronix 2232). The entire velocity-monitoring system is initiated (T_0) when a laser beam about 2 mm in front of the gun muzzle is occulted by the sabot slug extruding from the launch tube. Four additional laser/photodiode stations monitor the sabot pieces in free flight (providing times T_1, T_2, T_3, T_4), and an additional diode station monitors the light flashes of the sabot impacts (T_5). Generally, velocities deduced from times T_{1-5} agree with each other to <0.5%, and with the impact-flash data (t_x) to <1%, suggesting no measurable deceleration of the impactors at our typical chamber pressures of 1-2 x 10^{-3} torr. There is no capability to monitor the X/Y location of specific projectiles at the target front face, and specific impact features cannot be associated with a specific impact flash.

Two general types of oscilloscope records characterize the present experiments. The first and ideal type consists of sharp, clearly resolvable peaks, attesting to the arrival of a small number of projectiles, typically fewer than five. The arrival times of all projectiles are generally spread over ~30 μs, leading to <2% variance in velocity among individual impactors. The aerogel targets associated with such "good" records generally display a small number of well-defined tracks. The second type of oscilloscope record consists of a relatively broad hump of long duration, commonly >100 μs, that may or may not contain discrete spikes indicative of individual impactors. Invariably, the aerogel targets associated with such oscilloscope traces display numerous aerogel tracks of highly variable length. As a consequence, such records indicate the presence of a large number of very small projectiles that display a substantial spread in velocity that is as high as 20%, but more typically about 10%. Such prolonged and broad oscilloscope records, combined with the physical evidence in the aerogel targets, attest to pervasive fragmentation of projectiles during launch. Such records are the rule when launching powdered, natural materials and may even occur for some metallic aluminum projectiles at velocities above 6 km/s.

This breakup of projectiles takes place during actual light-gas gun launch where g-forces >10^6 g apply. Breakup seems unavoidable for projectiles manufactured by mechanical crushing of coarse raw stock, because such particles are invariably weakened by microcracks or deeper fractures. We expended considerable effort attempting to eliminate or decrease this projectile fragmentation by varying launch parameters such as the sabot material and length, sabot-cavity dimensions, number of projectiles, high-pressure diaphragm burst pressure, piston velocity, and initial driver-gas pressure without measurable success. In addition, we experimented with a number of fine-grained powders (<1 μm) that were mixed in variable weight ratios with the projectiles in an attempt to provide a cushion between neighboring grains; unfortunately, some powder would invariably cling to individual projectiles causing "compound" tracks unsuitable for calibration purposes. From these tests, we found that commercially available cocoa powder worked best (see Section 6). Shots were also

made with pure cocoa powder such that isolated clods impacted the aerogel targets, thus simulating impacts by relatively porous, fluffy particles of low-cohesive strength.

3.2 Aerogel Materials, Target Manufacture, and Particle Recovery

All aerogel materials used in this study were manufactured at the Jet Propulsion Laboratory, Pasadena, California (Hrubesh and Poco, 1990; Tsou, 1995). Typically, the aerogel was cast as tiles about 10 cm x 10 cm square and about 1 cm thick. The bulk density of aerogel is manipulated via the stoichiometric ratio of SiO_2 and solvent during aerogel manufacture. For our experiments, we determined the specific density of each tile by measuring and weighing each sample with an accuracy of no better than 10%, as tile thickness is difficult to measure and, on occasion, uneven. There is no detailed knowledge of possible density variations within a given aerogel tile, although some of our experiments suggest modest internal variations (as detailed below). An initial batch (Shipment I) of aerogel tiles consisted of 2.5-cm-thick monoliths ranging in density from 0.01 to 0.05 g/cm^3. These materials were used for the experiments assessing aerogel density, impact velocity, and a variety of projectile materials, including powdered chondrite meteorites Allende and Pampa-A. A second shipment (Shipment II) of aerogel consisted of material of nominally 0.02 g/cm^3 density; these materials were largely used for the oblique impacts and part of the cocoa shots. A third shipment (Shipment III), also of nominal density of 0.02 g/cm^3, was consumed during the experiments addressing the effects of collisionally disaggregated projectiles. As detailed below, distinction between these three shipments seems warranted.

Actual targets were typically 5 cm x 5 cm square after cutting the original tiles into four quadrants with a wire saw, which employed diamond-studded copper wire about 150 μm in thickness. This method allows reliable, rapid, and precise cutting without any lubricant or coolant, thus minimizing contamination. The sawed surfaces are rough, however, and of such decreased transparency that optical identification and measurement of penetration tracks becomes impractical.

Each target was placed into a dedicated, clear-plastic specimen box with the hinged lid removed (Fig. 1). Some spring-loaded, thin cardboard was first dropped into the empty box and the aerogel tile was placed on top of this platform, such that it modestly protruded above the open face of the specimen box. The plastic boxes were then placed into a cutout in the center of a Plexiglas disc, which constituted the interface with the remaining impact chamber hardware. The box is held in place by the protruding hinge knobs and the knob associated with the latching mechanism of the plastic boxes. This allows a spring-loaded frame, also made of cardboard, to push against the protruding aerogel until it is flush with the box opening. The spring-loaded frame and its tensioner screws (in corners) were mounted to a Plexiglas "hold-down frame" (Fig. 1) which, in turn, is mounted (two slotted, black screws) to the Plexiglas disc at a controlled distance. The entire device (Fig. 1b) is loaded into the gun's impact chamber. Following an experiment, the plastic box is removed from the target-holder disc and the lid of the plastic box is reattached; at this stage the target box becomes the long-term storage container for the aerogel target. Handling, viewing, and first-order optical inspection via binocular microscope are readily performed without removing the aerogel from the container.

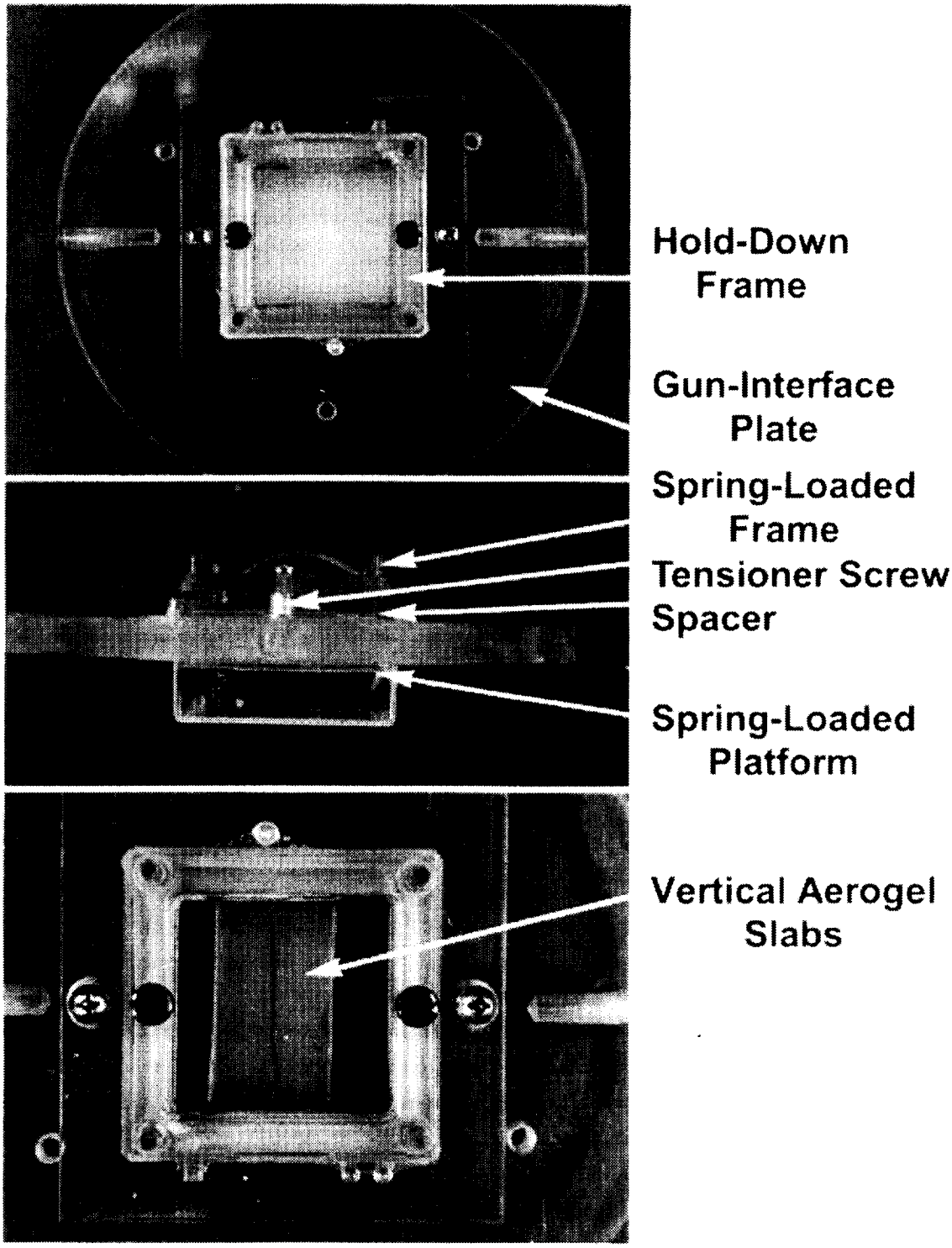

Figure 1a-c. Target assembly for aerogel experiments. Note the spring-loaded (lower) platform and (upper) frame in Fig. 1b; this arrangement permitted the aerogel sample to be firmly positioned so that the surface was flush with the opening of the plastic sample container. The overall arrangement provided for convenient and highly reproducible positioning of the aerogel target relative to gun axis. The large Plexiglas disk served as the interface with a target-mounting fixture inside the impact chamber.

Similar mounting procedures were used when vertically mounted slabs of aerogel were required (Fig. 1c), which was commonly the case when track length was expected to be deeper than the tile's original thickness. For such experiments, the 5-cm-x-5-cm tiles were cut in half, and the slabets were mounted on edge, thus resulting in targets ~2.5 cm thick. In such cases, two (Fig. 1c), three, or four such aerogel slabs were placed side-by-side inside the plastic box and held in place by multiply folded, springy cardboard.

These procedures were developed to permit fairly precise and reproducible cutting of large aerogel specimens, and to provide for easy manipulation of the delicate materials during a number of experimental steps, including reproducible mounting and orientation of the target relative to the gun axis and projectile path.

At the scale of the current experiments, many tracks measure 10 mm to 20 mm in length, and 1 mm to 3 mm in maximum width. As a result, it is possible to take a sharp razor blade, position it across the entrance hole of an experimental track, and split the entire target specimen along the defect represented by the track itself. While the track is not perfectly halved by this procedure, its interior is generally well exposed and amenable to detailed morphologic studies, including SEM analysis, without requiring additional sample preparation steps. Using this track-splitting method, any captured particle or its residue will reside at or very close to a freshly created, generally very transparent fracture surface. Consequently, the particle can be readily spotted under a binocular microscope and removed from the aerogel with a single-hair bristle.

We are confident that this *dry* recovery method will also work for large tracks in space-exposed collectors, yet there must be a size cutoff below which the splitting of individual, small tracks by razor blade will fail. This cutoff must be determined empirically for aerogels exposed on *Mir* and *Stardust*, as such a dry method of recovering projectile residue is extremely attractive from a contamination point of view, as well as being fairly rapid.

3.3 Projectile Materials and Properties

As previously mentioned, one of the most troublesome difficulties we encountered during experimentation is the breakup of some projectiles during launch. Projectiles, including our costly, commercially available, so-called precision spheres, vary in size, mass, and even shape. To minimize such effects, we routinely sieve (multiple times) the commercially acquired materials as well as those generated within the laboratory via grinding; sieves with mesh openings of 43 μm and 54 μm are used for this purpose. The inability to control and reproduce exactly the mass of what we refer to as 50-μm particles represents a serious handicap in establishing the precise, initial impact conditions on a particle-by-particle basis. Projectile radius may vary by factors of 1.25, implying mass variations of up to a factor of 2. In addition, detailed particle shape remains uncontrolled during sieving, yet it will substantially affect penetration processes (e.g., Hohler and Stilp, 1987; Orphal et al., 1990). To date, we have not conducted quantitative analysis of particle-size distributions and shape factors for our present projectile materials, as we are in the process of attempting to acquire superior materials to those presently in use. Regardless, we either suspect (e.g., Burchell and Thompson, 1996; see below) or know (e.g., Barrett et al., 1992) that uncertainties in the initial impactor conditions can greatly affect the experimental results (i.e., track length, recovered projectile mass, etc.).

The rationale for actual selection of projectile species is given below, together with some photodocumenta-tion of typical projectile sizes and shapes. In addition, some brief evaluations concerning the ease of projectile fragmentation at 6 km/s are given, loosely defined as event rate per individual gun firing. A "nominal" event implies a straight, slender track that contains clearly discernible residue at the terminus; as discussed below, they are usually differentiated from possible background tracks that formed by projectile fragments and/or the occasional gun debris.

3.3.1 Aluminum, Metal (Fig. 2a)

The rationale to experiment with metallic aluminum relates to the*Mir* objective of characterizing structurally disintegrated metallic aluminum. It is also a metal that is well-characterized in terms of physical properties for modeling purposes. Among a variety of commercial products, we selected Al_{2024} spheres on the basis of uniform size and relatively uniform, smooth surface. Nevertheless, some ellipsoids are present, along with (rare) compound particles that consist of numerous smaller particles welded together.

In general, aluminum can be launched at velocities below 5 km/s without difficulty, while some modest projectile breakup may occur above 5 km/s, becoming much more common at 6 km/s. During a typical experiment, the collection of projectiles will consist of 50 to 80 projectiles loaded into the sabot, which typically yields 2 to 5 projectiles on target.

3.3.2 Aluminum, Oxide (Al_2O_3; Fig. 2b)

Precision ruby spheres, 130 μm in diameter were selected and acquired in direct support of ODC. Clearly, this material is of great theoretical interest, as its high melting temperature and compressive strength render it highly suitable to study penetration processes of unfragmented impactors that may not have suffered extensive ablation. Among the diverse projectile materials tested, Al_2O_3 is the most refractory and should be the least modified during penetration.

Considerable effort was made to obtain suitable 50 μm Al_2O_3 spheres; unfortunately, this effort was unsuccessful. In addition, we evaluated diverse grinding materials, but these were disqualified due to extreme variation in particle shape; powdered corundum (Fig. 2b) was deemed unsuitable for this reason. The use of solid-fuel rocket exhaust products as projectiles was explored, but most of those particles >20 μm in size are typically compound, sintered, highly heterogeneous aggregates.

High quality (dimensions and purity) Al_2O_3 spheres 130 μm in diameter are readily launched, typically yielding more than two events per experiment on target. When testing powdered corundum, we observed projectile breakup, demonstrating that crushing via pestle and mortar generates penetrative cracks in most materials, causing individual particles to fail during launch.

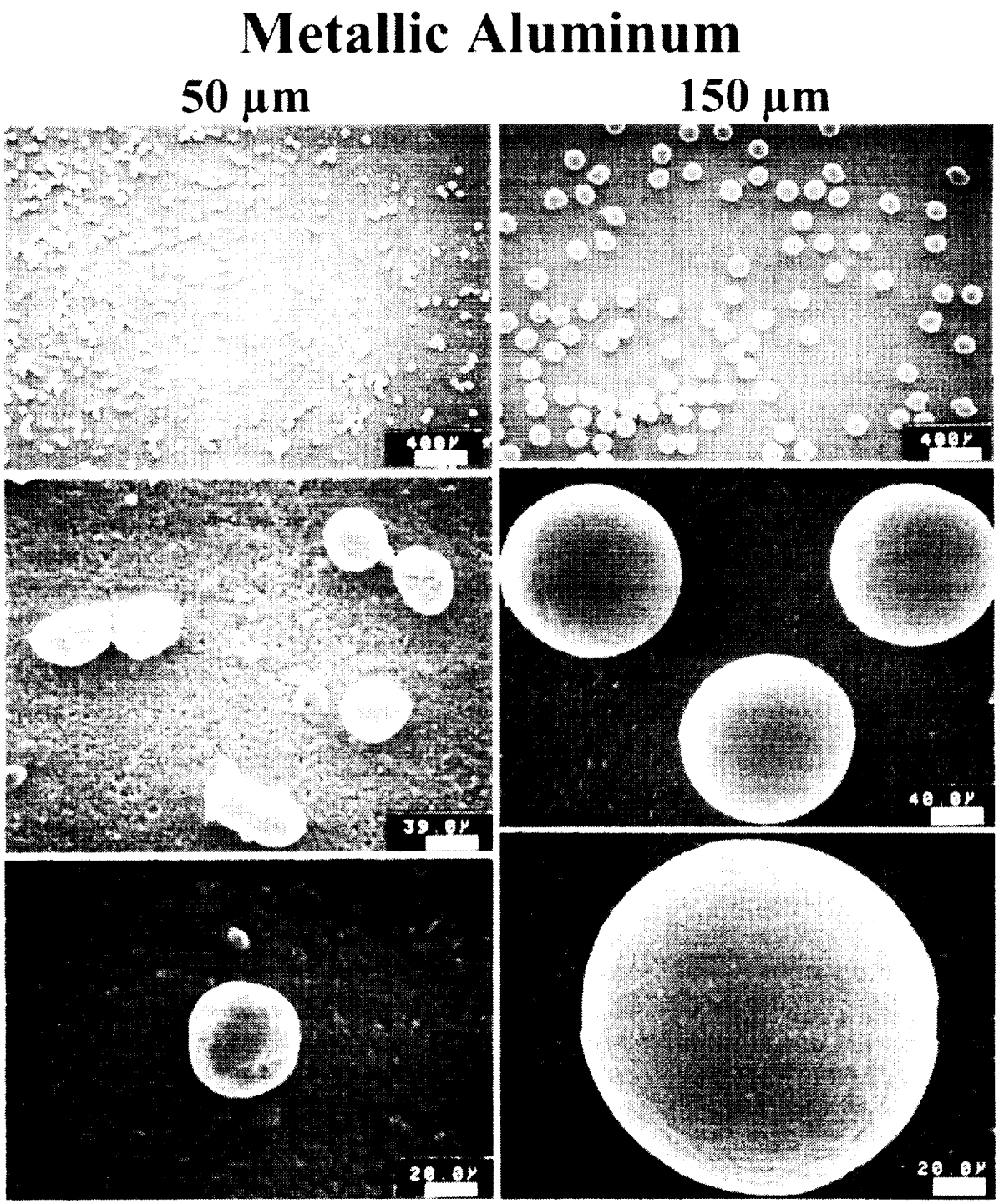

Figure 2a. SEM photographs of the projectiles available for the present study, as well as that of Barrett et al. (1992). Note the differences in size and shape between these carefully sieved materials, especially those that were manufactured by crushing: (a) Metallic aluminum, series 2024, (b) aluminum oxide, (c) soda-lime glass, (d) olivine, (e) pyrrhotite, (f) Allende meteorite, (g) Pampa-A meteorite, and (h) powdered soda-lime glass.

Aluminum Oxide

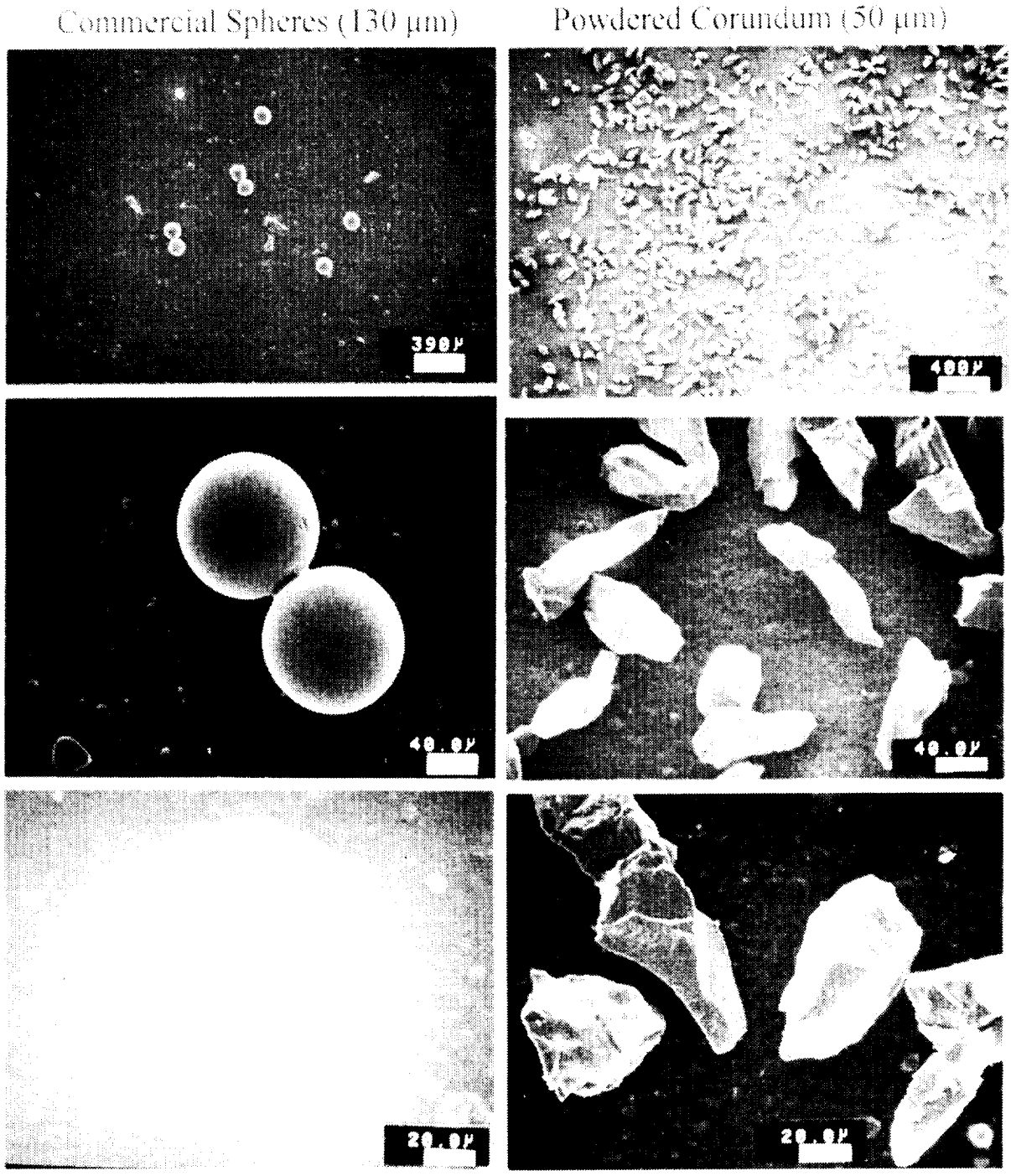

Figure 2b. SEM photographs of aluminum oxide.

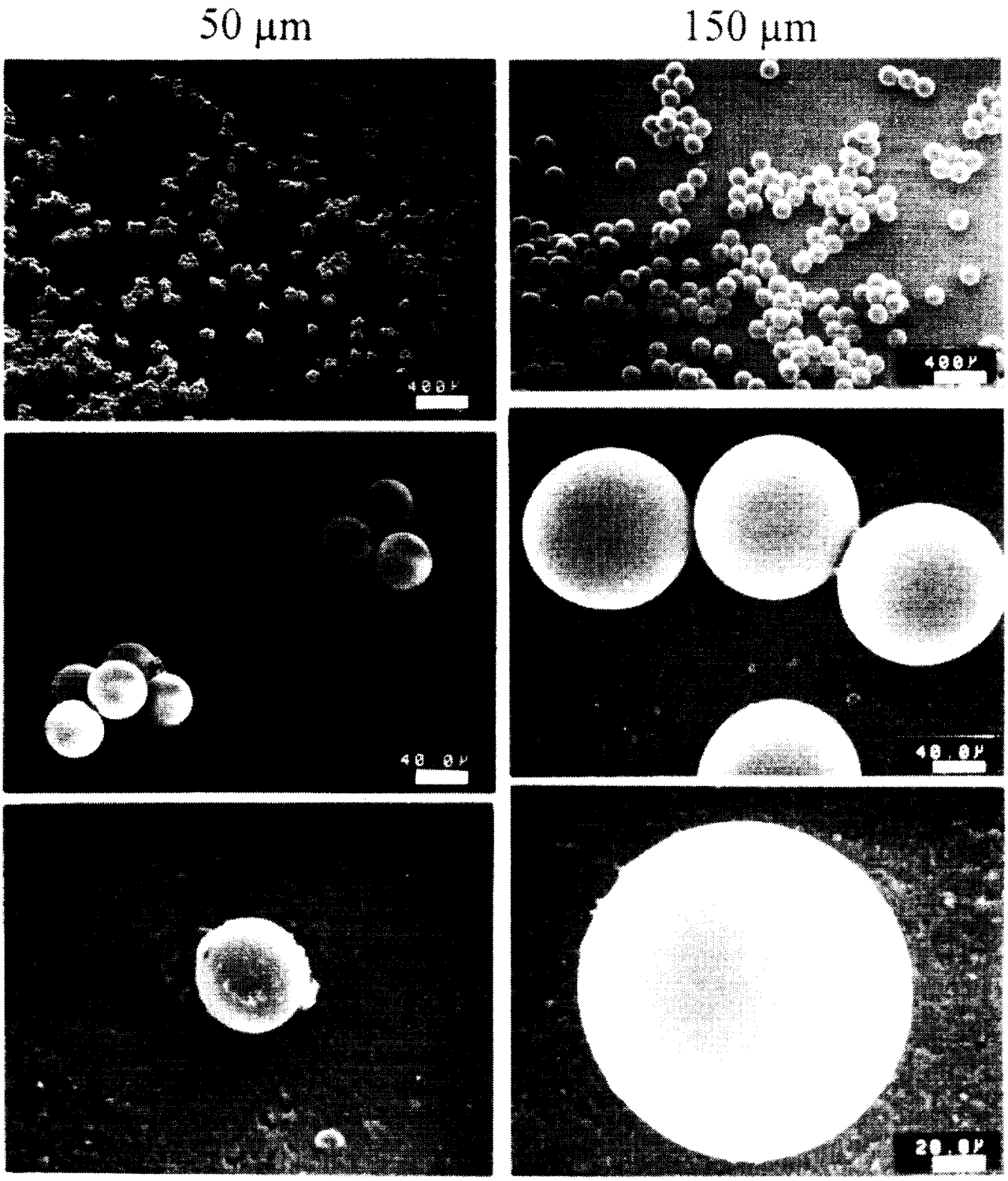

Figure 2c. SEM photographs of soda-lime glass.

3.3.3 Soda-Lime Glass (Fig. 2c)

The anticipated comparisons in the penetration behavior of metals, oxides, and silicates necessitated a spherical silicate. We obtained precision spheres of soda-lime glass (Fig. 2c); even such materials contain a fair number of ellipsoids and non-spherical particles, or spheres that display internal flaws and accretionary microspheres. For the purposes of some select calibration shots, such flawed spheres were culled under the optical microscope. Soda lime is the best spherical silicate we were able to find.

Soda-lime glass spheres are easily launched (more than two impacts per experiment) over the full range of velocity (3-7 km/s), yet occasional breakup of individual particles, most likely flawed by vesicles or microcracks, is unavoidable. Clearly, this projectile species represents the best silicate to be launched, as our other silicates consisted of powders crushed from coarse raw stock.

3.3.4 Olivine (Fig. 2d)

Olivine ranks among the most abundant rock-forming minerals in extraterrestrial materials. Polycrystalline dunite (99% olivine, from Twin Sisters, Washington) was ground in a mortar and repeatedly sieved. As illustrated in Fig. 2d, particle shapes and masses vary considerably. Among all natural materials used, this material may be viewed as an endmember in terms of physical toughness and resistance to fragmentation and comminution (Cintala and Hörz, 1992).

Olivine fractures noticeably during launch at all impact velocities; up to 6 km/s the total yield of nominal particles averages better than one event per experiment, second best for all silicates in our projectile inventory.

3.3.5 Pyrrhotite (Fig. 2e)

A number of single-crystal pyrrhotites were generated via grinding and, despite repeated sievings, the particle shapes and masses vary considerably (Fig. 2e). This material represents abundant Fe-S-phases in comic-dust and meteorite specimens. It seemed particularly suited to reveal potential, selective loss of relatively volatile S in the captured residues, thereby illuminating details of the thermal environment during aerogel penetration and th-e potential loss of elements by selective volatilization. At 6 km/s, pyrrhotite breaks up more readily than olivine, yielding, on average, one nominal event per experiment.

Powdered Olivine

50 μm

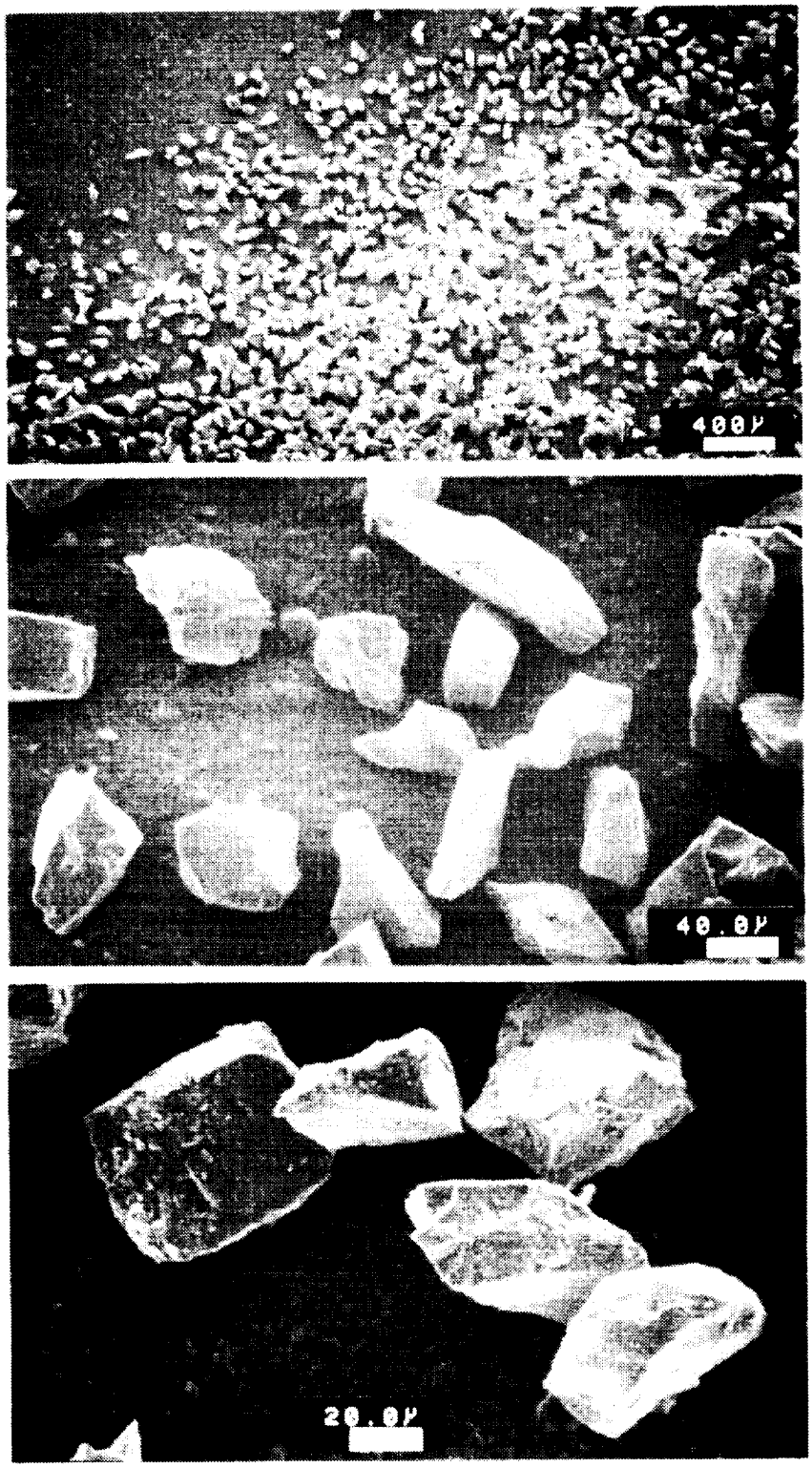

Figure 2d. SEM photographs of powdered olivine.

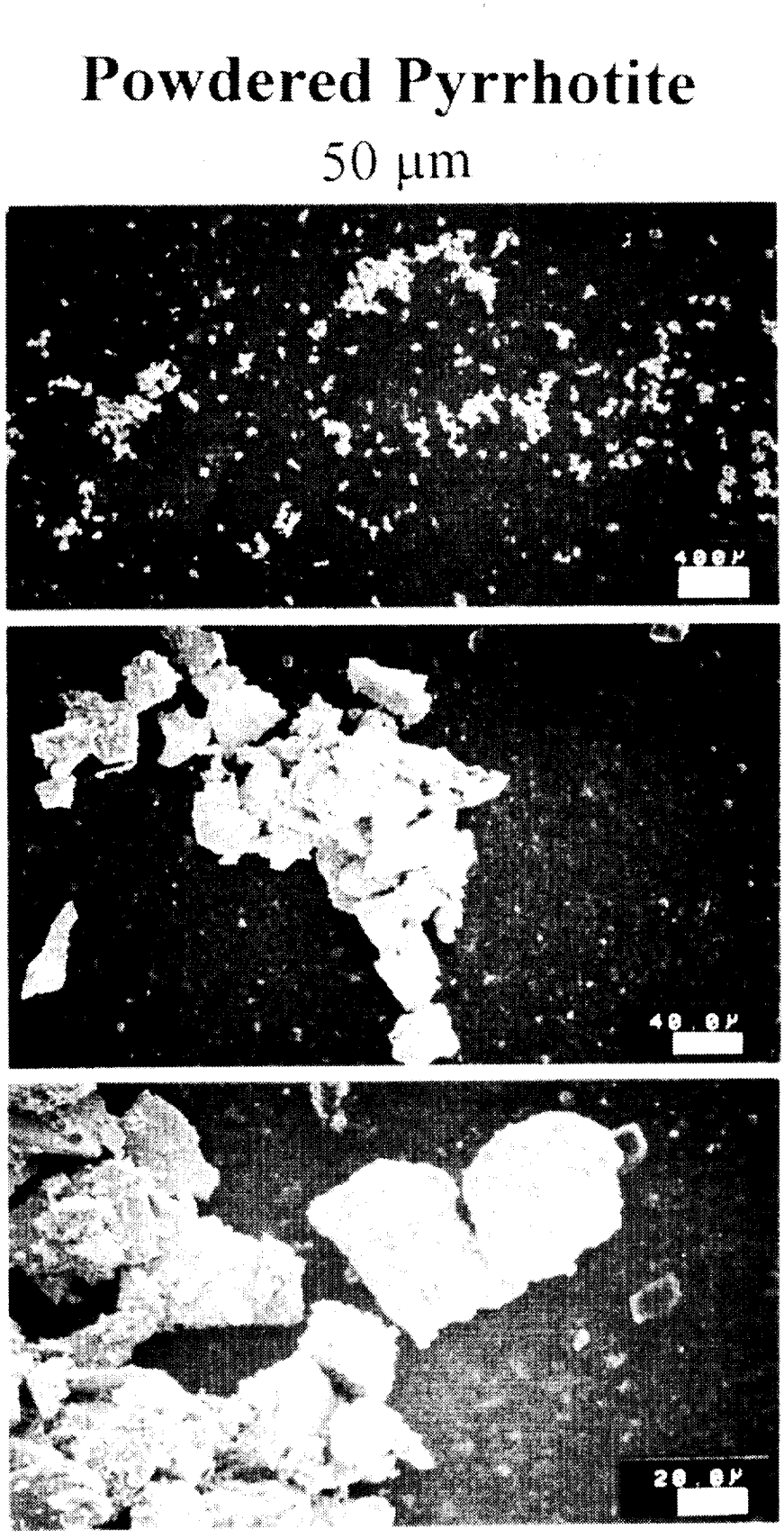

Figure 2e. SEM photographs of powdered pyrrhotite.

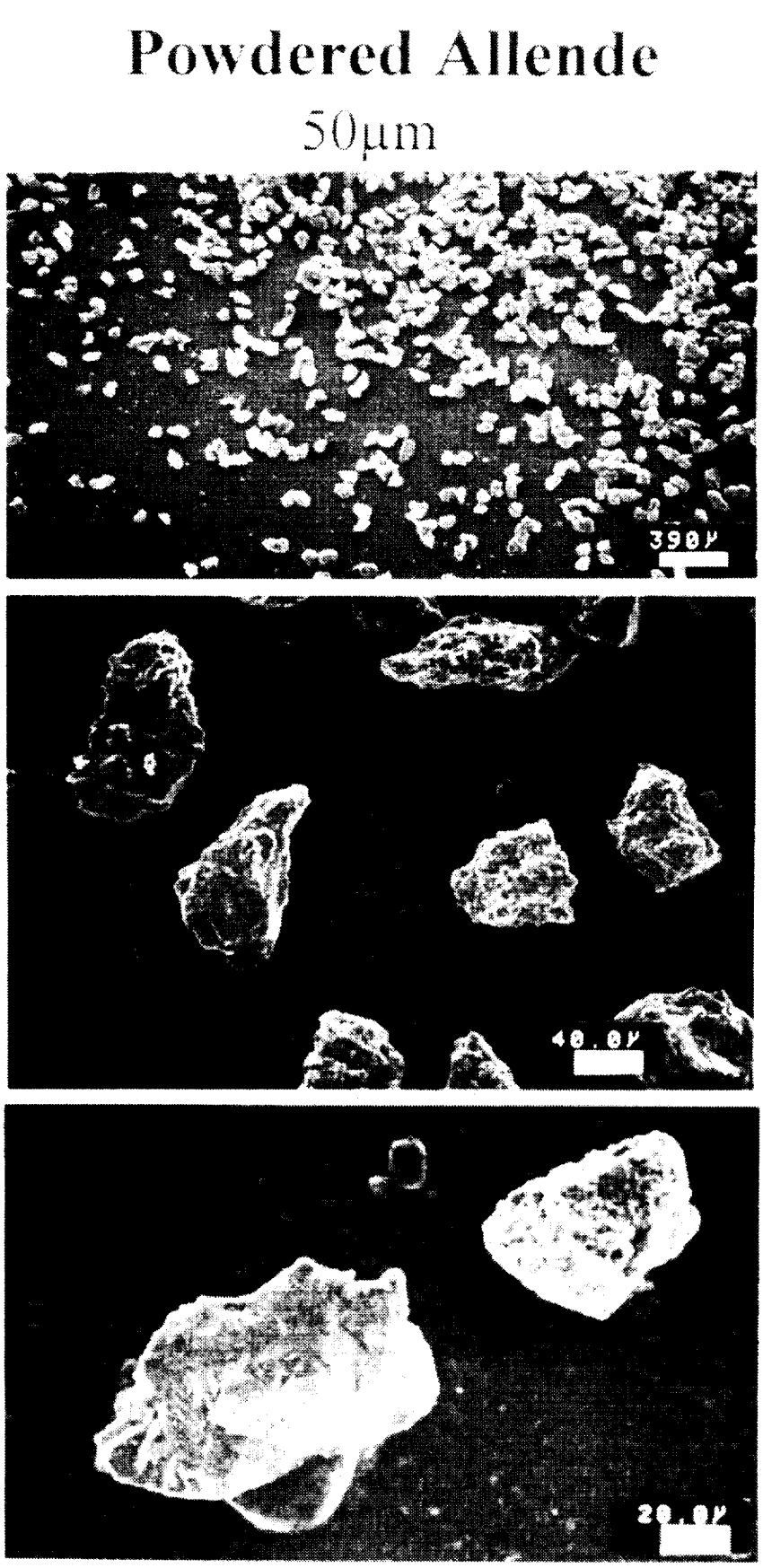

Figure 2f. SEM photographs of powdered Allende meteorite.

3.3.6 Allende (Fig. 2f)

Chunks of the Allende meteorite, a carbonaceous chondrite, were ground in the laboratory and, despite repeated sieving, the particle size and shape varied considerably (Fig. 2f). In addition, the mineralogical mode seemed to vary from grain to grain, consistent with the modal abundance and grain-size distribution of component minerals, chondrules, and matrix. This Allende powder must be considered a high-fidelity mineralogical analogue to prospective natural particles; as meteorites go, Allende constitutes a moderately tough rock.

Powdered Allende samples are difficult to launch at all velocities, and most mass loaded into the sabot cavity breaks up; an average of all experiments yields less than one nominal impact per experiment.

3.3.7 Pampa-A (Fig. 2g)

Pampa-A is another ordinary chondrite that was ground into projectile material; it is noticeably more compact and tougher than Allende. The idea was to attempt to generate projectiles that would not fragment during launch. As illustrated (Fig. 2g), particle shape and size varied considerably.

Powdered Pampa-A is similar to Allende in launch characteristics, typically yielding less than one nominal impact per experiment.

3.3.8 Powdered Soda-Lime Glass (Fig. 2h)

We have not yet experimented with this material, but we are considering it and the powdered corundum of Fig. 2b to assess the effects of projectile shape on penetration depth. These two powders will be paired with observations from spherical impactors to illuminate the effects of particle shape.

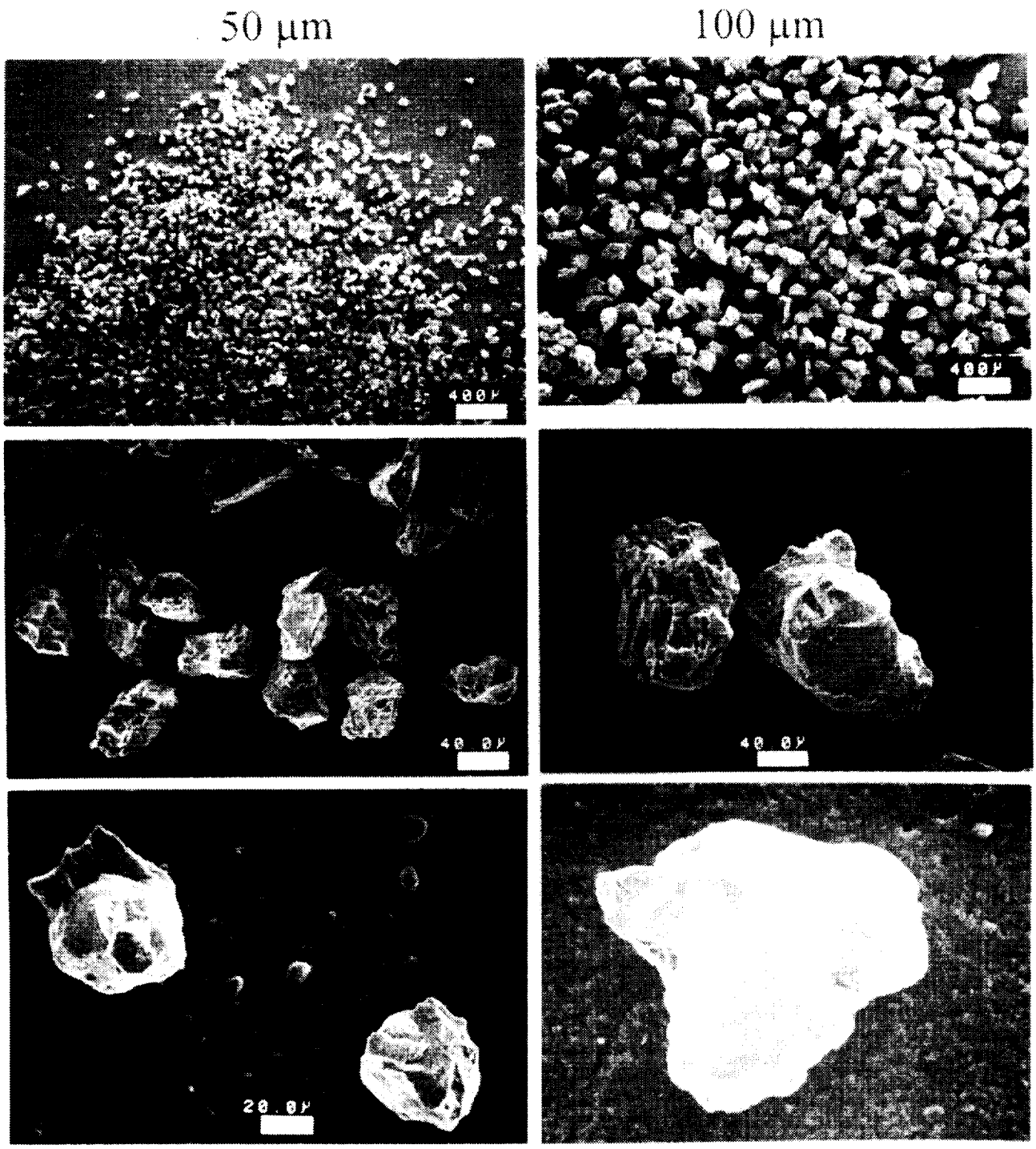

Figure 2g. SEM photographs of Pampa-A meteorite.

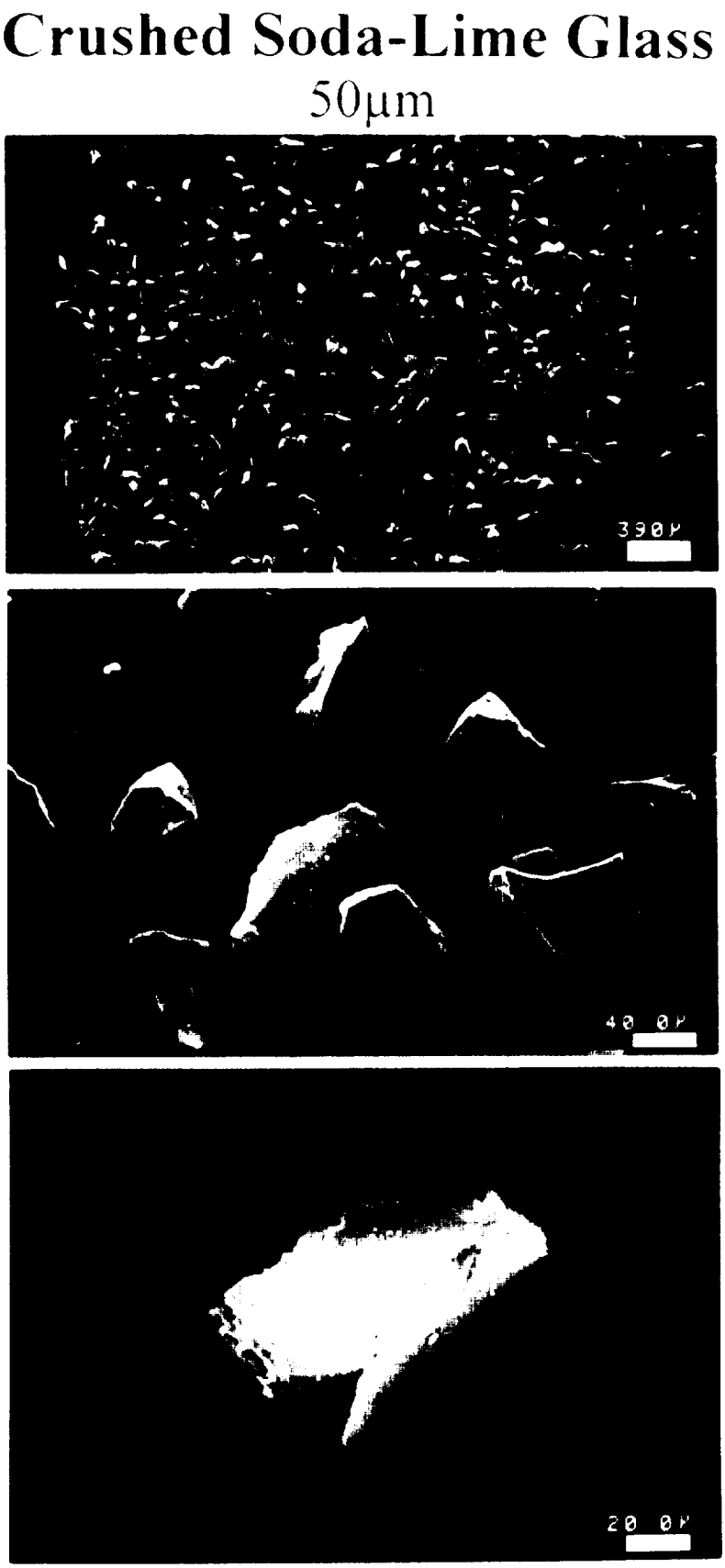

Figure 2h. SEM photographs of powdered soda-lime glass.

4. Impact Experiments at Normal Incidence

This section describes the experimental series aimed at evaluating the effects of aerogel density on track length, and especially on mass loss of the projectile during hypervelocity capture. The experiments of Barrett et al. (1991) that used aerogel densities of 0.02and 0.04 g/cm^3 suggested superior residue recovery compared to the 0.12-g/cm^3 case. Thomson (1995) also employed relatively high-density aerogels (0.09 and 0.12 g/cm^3), recovering, at best, about 10% of the initial impactor mass. The present tests concentrate on aerogels with densities below 0.050 g/cm^3, with the majority of experiments conducted at 0.02 g/cm^3. All aerogel specimens for this series were exceptionally clear and homogeneous materials (Shipment I), with nominal densities of 0.050, 0.040, 0.035, 0.020, and 0.010 g/cm^3. Figure 3 illustrates the experiment matrix for this particular series; note the extensive experimentation with aerogel of 0.02 g/cm^3 density (in part from Shipment II), the density of the exposed aerogel collectors on *Mir*.

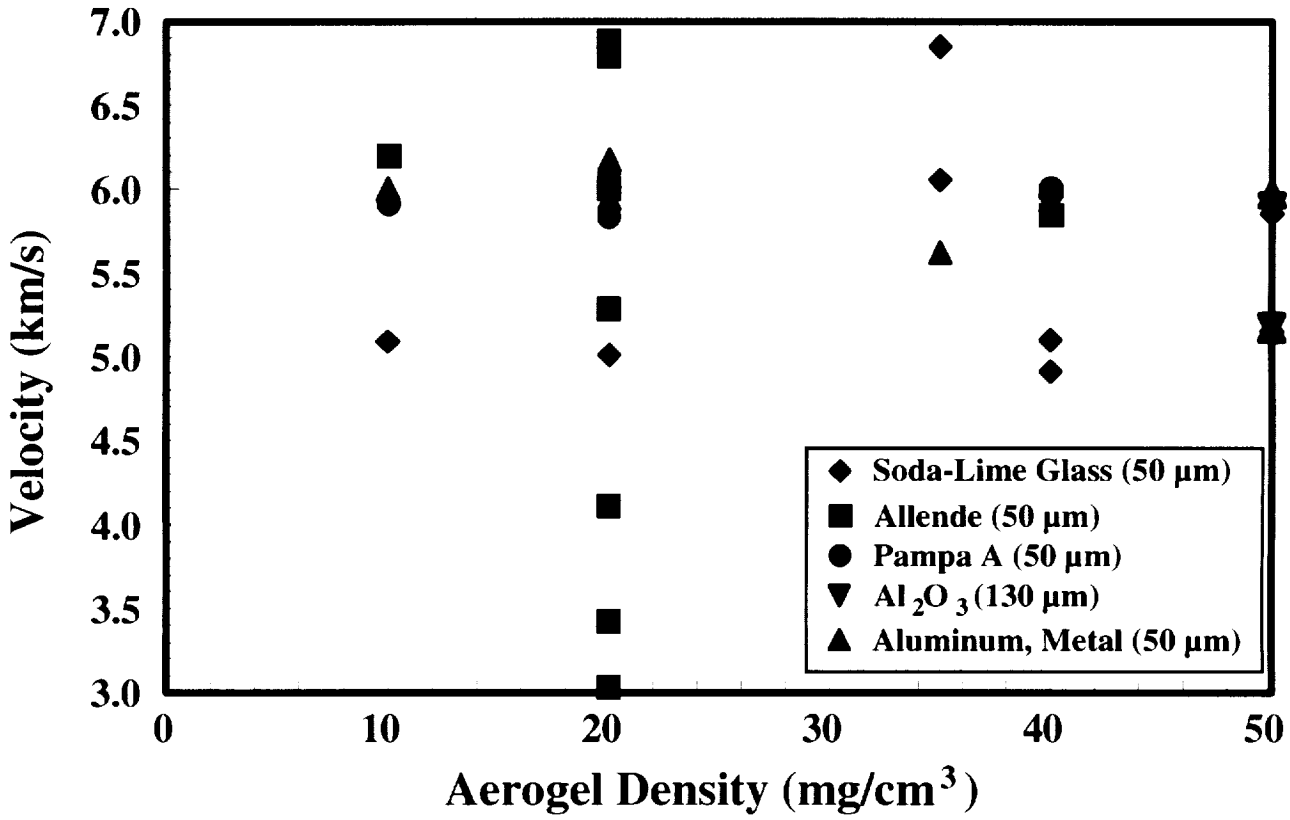

Figure 3. Plot outlining the experiment matrix of the initial series of tests, the primary purpose of which was aimed at an improved understanding of the effects of aerogel density and impact velocity on absolute penetration-depth and mass of the recovered residue.

Figure 4a presents typical penetration tracks as a function of aerogel density produced by soda-lime glass spheres at velocities near 6 km/s. Note the systematic dependence of track length on aerogel density. The morphologies of such tracks were extensively described by Barrett et al. (1992), Mendez (1994), and Thomson (1995), and are similar to those observed in porous alumina (Werle et al, 1981) or Styrofoam

(Tsou, 1990). There appears to be nothing unusual about tracks produced in very low-density aerogels compared to published observations, except for the distinctly "stepped" tracks in the 0.01 g/cm^3 case. The latter tracks repeatedly change their diameters with depth into the target in rather abrupt fashion, a seemingly unique and previously unreported phenomenon for which we have no ready explanation. Figures 4b and 4c illustrate typical tracks for impacts by powdered Allende and Pampa-A projectiles, respectively. Note that Figures 4a-4c are reproduced to approximately the same scale and that the natural impactors generate somewhat shorter tracks than the glass spheres.

We also observed bifurcation, if not multiple splitting of some tracks as previously reported as "starburst" tracks by Thomson (1995); good examples are illustrated in Figure 5, using Pampa-A projectiles. Obviously, such tracks reflect breakup of projectiles, typically in the early stages of penetration, but occasionally at late stages as well. Such split tracks are fairly common for the powdered meteorite projectiles, but they are absent in the case of soda-lime glass, metallic aluminum, and aluminum-oxide spheres. Track splitting seems to suggest projectile failure along microcracks that were introduced either during projectile manufacture or launch. Invariably, targets containing split tracks also display a substantial population of relatively short tracks, indicative of projectile fragmentation during launch.

Some minor tracks are visible even in the case of soda-lime glass spheres (e.g., the 0.02 g/cm^3 case in Figure 4a). Such small tracks seem unavoidable and result from particulate contaminants such as gun-barrel abrasion products and particles shed from the bursting of the high-pressure diaphragm or the high-pressure piston; they could also represent ejecta generated during sabot impact. Such contaminants can occur over a wide range of sizes. Debris much smaller and, on rare occasions, much larger than the nominal impactors is readily spotted by absolute track length. Contaminants producing tracks of expected nominal dimensions, not to be confused with the nominal projectile impact, are invariably associated with a detectable population of small debris tracks. Nevertheless, optical or chemical characterization and identification of the impactor residue is necessary to positively differentiate between tracks resulting from nominal projectiles and those produced by undesirable contaminants.

The optical photographs presented in Figure 4 do not portray the target surfaces in great detail. Nevertheless, it seems obvious that all tracks in <0.05 g/cm^3 aerogel lack the substantial spall zones that are so prominent in 0.09 g/cm^3 aerogel, as detailed by Thompson (1995) and Burchell and Thomson (1996). Indeed, most shots into 0.01 and 0.02 g/cm^3 aerogel display a rather crisp and small entrance hole without any spallation features. Immediately below the surface, the penetration track rapidly grows into a bulbous shape, from which it gradually tapers off to form the typical slender, carrot-shaped track. Also note a few modestly curved tracks and those of apparently oblique orientation relative to the aerogel surface for the powdered meteorites; in comparison, the tracks formed by regular spheres tend to be straight. We ascribe the curvature and deviation from normal-incidence angle of the Allende and Pampa-A tracks to irregular projectile shapes that result in uneven drag forces during deceleration.

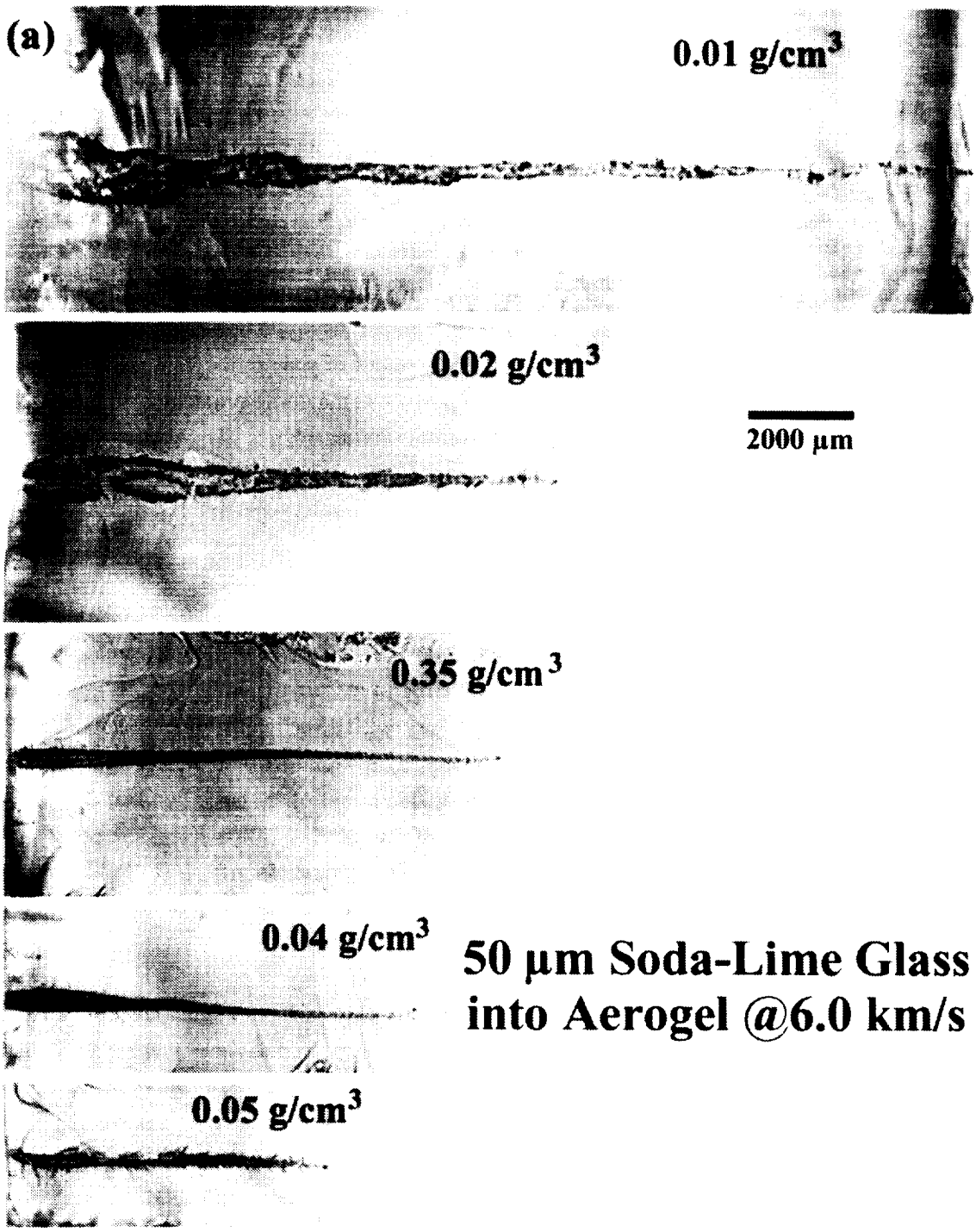

Figure 4a. Optical photographs of penetration tracks created by 50-μm impactors in aerogel targets of different density. (a) Spherical soda-lime glass projectiles, (b) powdered Allende projectiles, and (c) powdered Pampa-A projectiles.

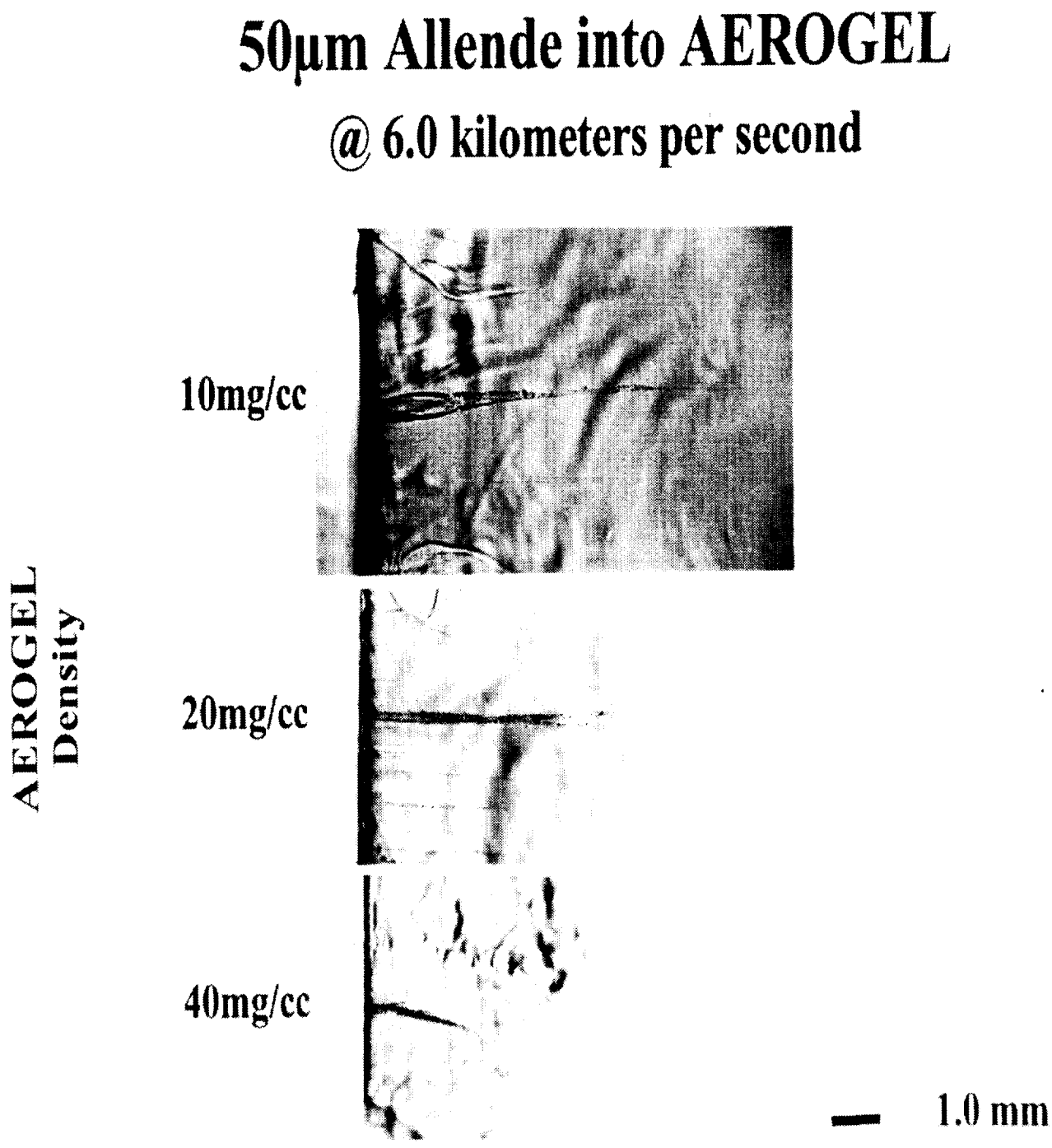

Figure 4b. Penetration tracks of powdered Allende projectiles.

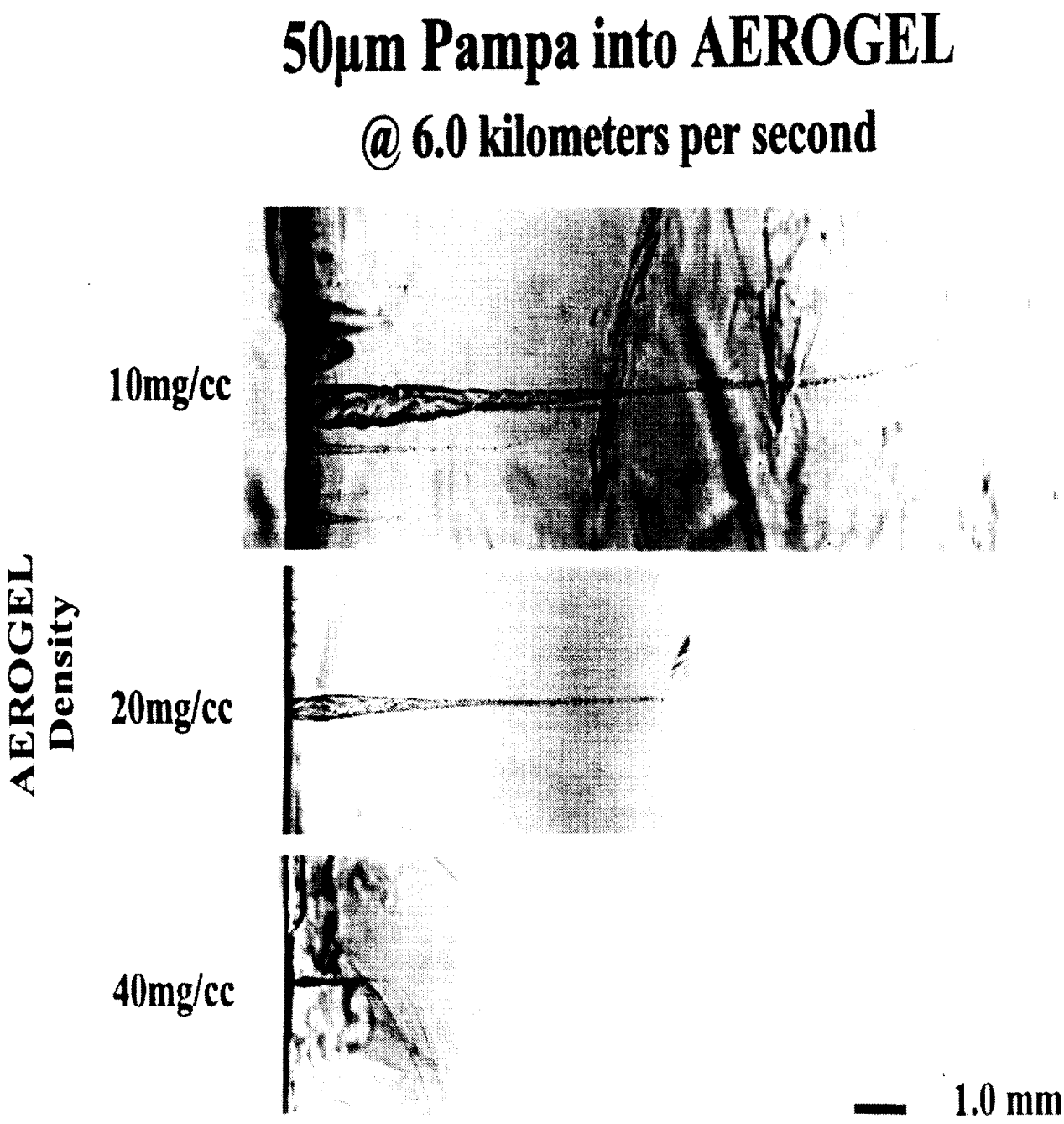

Figure 4c. Penetration tracks of powdered Pampa-A projectiles.

Figure 5. Bifurcated tracks caused by a 50-µm Pampa-A projectile impacting at about 6.0 km/s. Note the presence of a third track, in the top view, that is partly obscured behind the track in the foreground. Dark residue is visible at the end of most tracks, which tend to curve gently as the projectile decelerates.

The track lengths at a constant 6 km/s—normalized to projectile diameter—are plotted as a function of aerogel density in Figure 6a, while absolute track lengths of the silicate impactors only are detailed in Figure 6b. There is substantial variation among the five projectile materials employed. Not surprisingly, Al_2O_3 seems to penetrate the deepest, as it is not only the highest density impactor, but also the one characterized by the highest melting point and compressive strength. Soda-lime glass penetrates with almost the same ease as Al_2O_3, followed by metallic aluminum, and the powdered meteorites, with Pampa-A penetrating modestly deeper than Allende. The relatively poor penetration power of metallic aluminum is somewhat surprising, yet it is the most malleable material employed in this study, as well as that with the lowest melting point, so it most likely suffers the most deformation and/or ablation during capture.

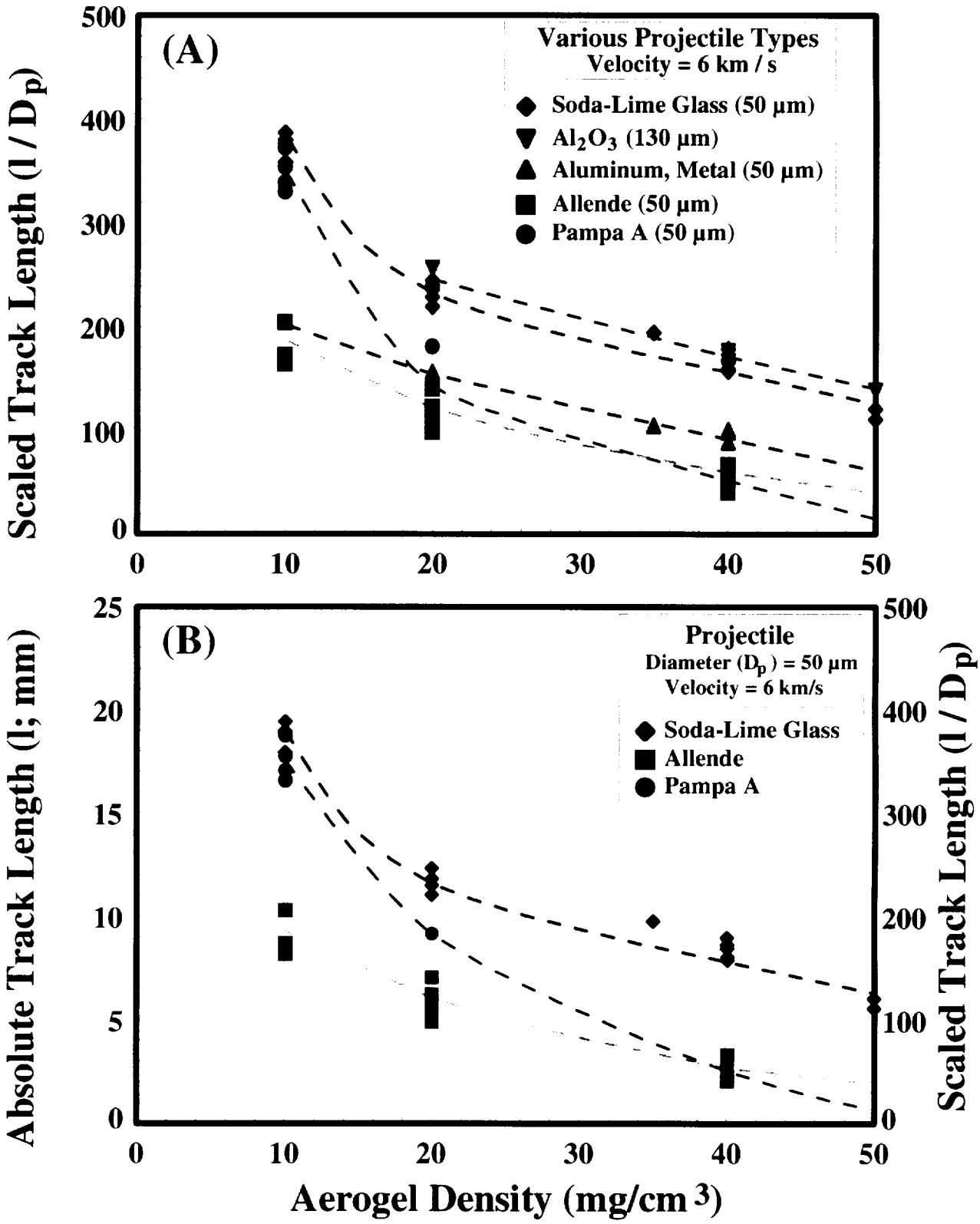

Figure 6. Track length plotted as a function of aerogel density; projectile velocity remained constant near 6 km/s while the projectile types were varied. (a) Track length (l) normalized to the nominal projectile radius (D_p = 50 µm) and (b) absolute track length for the 50-µm silicate impactors only. Note the apparently good reproducibility of track length for any given initial condition (see text).

Clearly, all materials display the same trends, albeit to various degrees, of having increasingly deeper penetration with decreasing aerogel density. There is tentative evidence that a particularly significant change in penetration capabilities occurs between 0.01 and 0.02 g/cm^3, as detailed via Figure 6a. Based on the experimental difficulties and uncertainties afflicting these experiments, more rigorous interpretations of Figure 6 do not appear warranted at this stage.

The velocity dependence of penetration depth in aerogels of variable densities was investigated with 50-μm soda-lime glass spheres. The results for 5 and 6 km/s (±0.1 km/s) are illustrated in Figure 7. Obviously, the 5 km/s impactors penetrate deeper than those at 6 km/s under all experimental conditions, a result that appears consistent with the penetration experiments using porous alumina by Werle et al. (1981) and low-density polymer foams (Tsou, 1990). The latter studies report an optimum penetration depth in these highly porous targets at relatively modest velocities (<5 km/s).

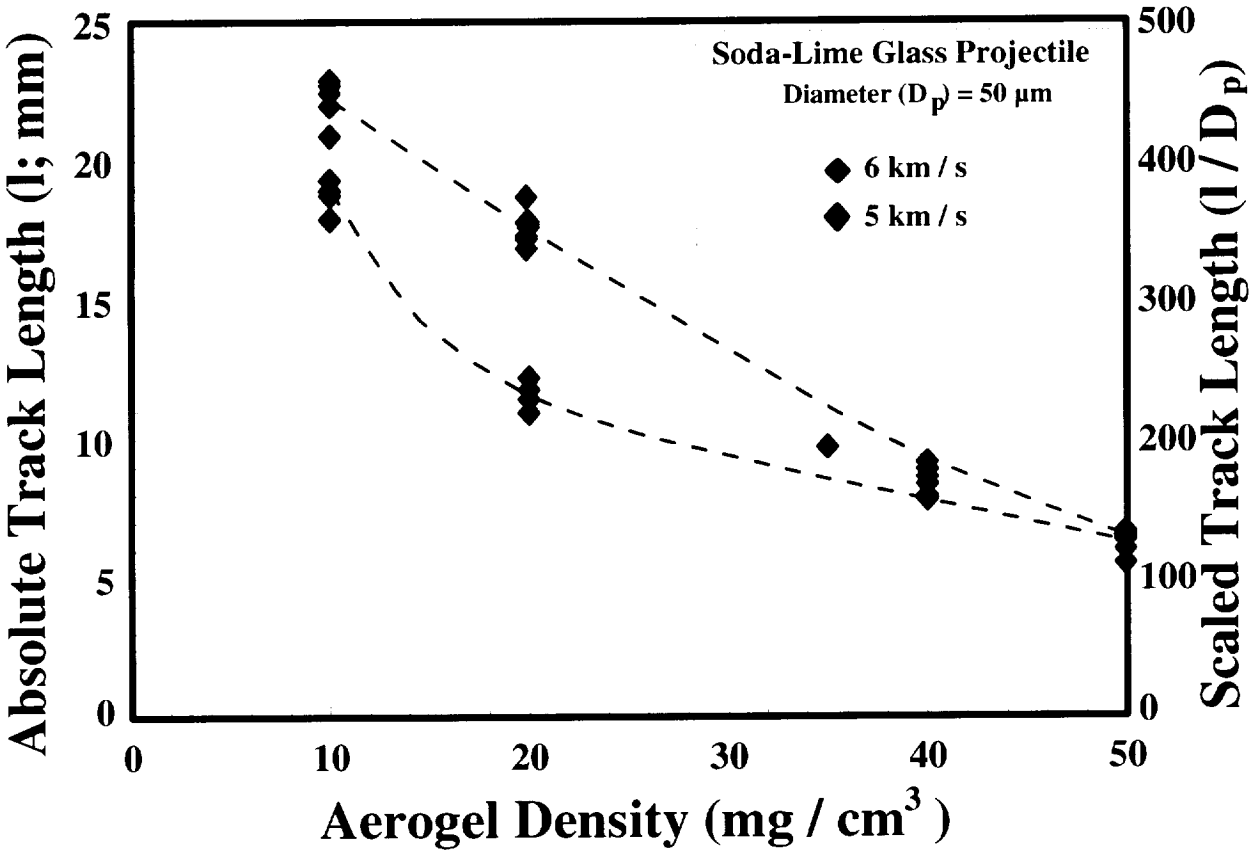

Figure 7. Track length in aerogels of different density produced by 50-μm soda-lime glass spheres at 5 and 6 km/s; note that some of the data result from duplicate experiments (see text).

A major reason for presenting the above dimensional data is to illuminate the reproducibility of aerogel penetration tracks under presumably controlled laboratory conditions. The reproducibility is poor, at present, for the various experimental reasons outlined above (see also Thomson, 1995, and Burchell and Thomson, 1996). Substantial differences in track length seem unavoidable when experimenting with very small projectiles that are sized by sieving. Referring only to the soda-lime glass shots (e.g., in Figure 6b), the present data tend to group in much tighter clusters than those of Thomson (1995) and Burchell and Thomson (1996). In particular, we emphasize that the 0.01 and 0.02 g/cm^3 data each refer to two repeat experiments, attesting to good reproducibility of track length from experiment to experiment. Good reproducibility of track length is portrayed in Figure 6b as well, which includes the Allende and Pampa-A projectiles, with the Allende data at 0.02 g/cm^3 being the composite of two experiments. While there are not very many individual experiments that produced multiple tracks with the Al_2O_3 and metallic aluminum projectiles, the trends displayed in Figure 6a also seem sufficiently systematic to suggest much less data scatter than that reported by Thomson (1995) and Burchell and Thomson (1996).

The apparent tighter clustering of data points in Figure 6 relative to those of Thomson (1995) or Burchell and Thomson (1996) is real for the unbroken projectiles (glass, Al, Al_2O_3), yet it is an artifact for the meteorites. The meteorite data are the result of subjective classifications of an observable track population into good and bad tracks, the latter unplotted. Figure 8 (unlike Figures 4b and 4c) illustrates typical target scenes employing Allende (Figures 8a and 8b) and Pampa-A (Fig. 8c) projectiles. First, note the very large number of tracks per any individual experiment, clearly the first sign and telltale evidence that projectile fragmentation during launch may have occurred. It seems self-evident that the large number of small tracks must be assigned to small-fragment impacts, and only some of the largest tracks may be assigned to nominal impactors near 50 μm in size. Figure 8a contains two tracks that are about 1/3 the length of the longest nominal track, and we consider them to be the result of projectile fragments. Figure 8b illustrates the common and more ambiguous case, in which a number of tracks are on the order of the longest track, consistent with expected mass variations of the projectiles. Recovery of projectile residues identified them as meteorite fragments; we consider them to be nominal and plotted those data in Figure 6. Somewhat shorter tracks are also present in Figure 8, yet their interpretation was ambiguous, so they are not plotted in Figure 6. Figure 8c illustrates a single nominal track (towards top) that terminates outside the image and a second, major track (towards bottom) that terminates close to the image's edge. Although of different length, both tracks may represent nominal impactors, given the variation in mass of the sieved projectile ensemble. Both of these long tracks are readily contrasted with a population of smaller tracks of variable lengths, all of which were assigned to fragment origins.

On the basis of these examples, recognition and subsequent elimination of unsuitable tracks can be a difficult judgment call that varies from target to target. Fortunately, in the majority of cases there are a small number (2 to 5) of the longest penetrations, all within 10% to 20% in absolute length, that contrast markedly with a fair number of tracks that are typically less than half the length of the longest tracks. Nevertheless, classification as a nominal track and elimination of the remaining population remains subjective in a significant number of cases. In addition, there is no independent evidence or guarantee that any nominal track is indeed the product of a nominal meteorite projectile; the latter assignment rests, in large part, on comparative data with unbroken glass projectiles.

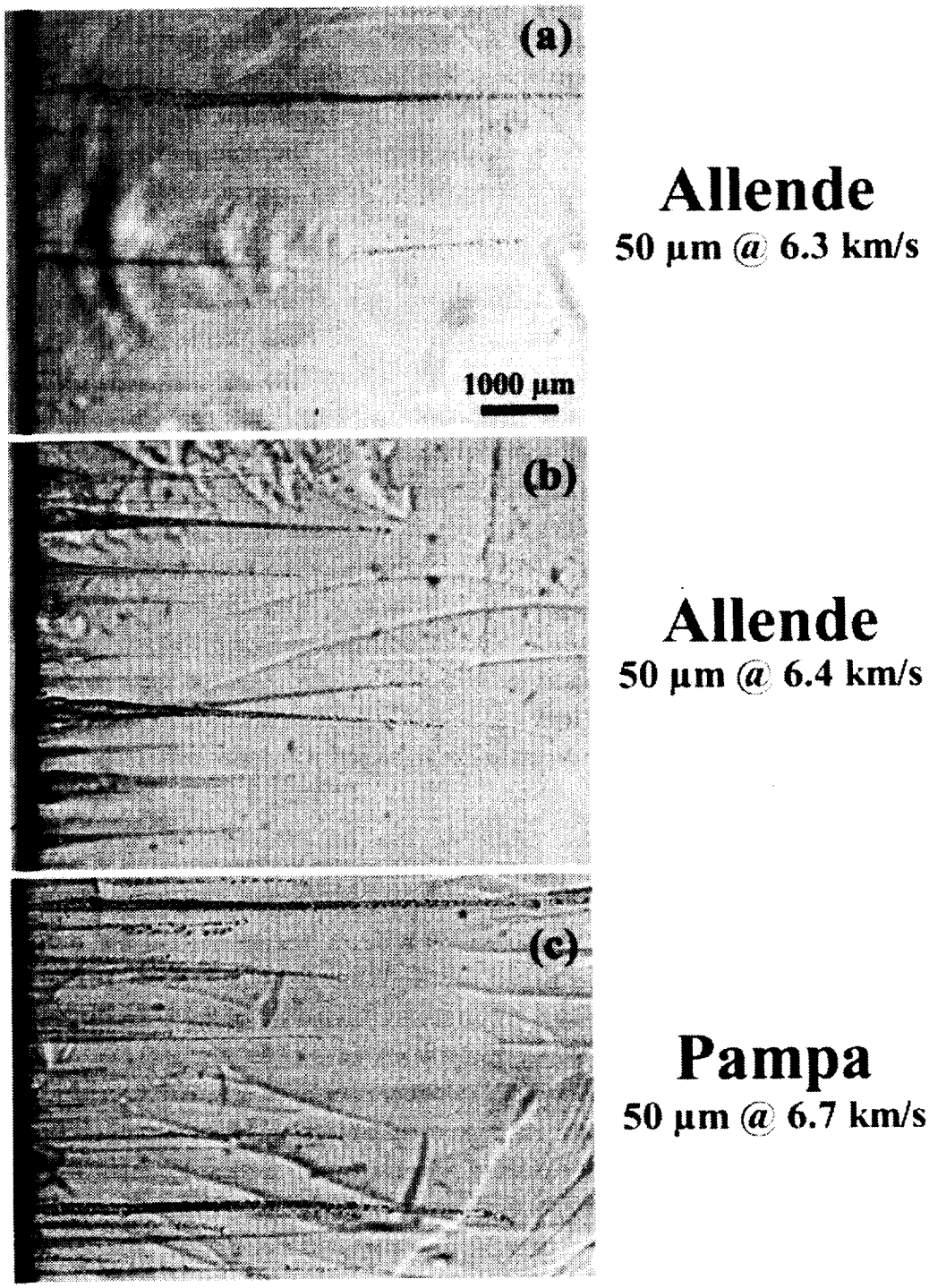

Figure 8a-c. Typical populations of penetration tracks in 0.02-g/cm^3 aerogel resulting from the impact of 50-µm particles of powdered meteorite. Samples shown in photographs (a) and (b) are tracks resulting from Allende projectiles with velocities of 6.3 and 6.4 km/s, respectively, while (c) shows tracks from Pampa-A particles (6.7 km/s). While qualitative, these photographs serve to illustrate that projectile breakup is more severe at higher velocities and accelerations than at lower velocities. Some tracks exhibit slight curvature toward the end, suggesting the presence of irregular grain shapes.

When severe, launch-induced projectile fragmentation occurs, track classification is much more difficult, and none of the tracks can be considered representative of nominal impactors. Such is the case at high impactor velocities, which are invariably characterized by a very large population of small tracks. The positive recognition of an unsuccessful experiment on the basis of an anomalous oscilloscope record and an unusually large population of short tracks justify rejection of such experiments. Therefore, the meteorite data illustrated in Figures 6 and 7 refer only to the few, longest tracks for any given target that also contained relatively massive impactor residues.

One way of conveying these experimental and interpretational difficulties is illustrated in Figure 9. Figure 9a plots track length against impact velocity for seven experiments using Allende projectiles and aerogel of constant density (0.02 g/cm^3). The observed population of tracks was classified into (a) tracks >5 mm in length, (b) tracks between 3 and 5 mm, and (c) tracks <3 mm long. Figure 9a portrays all tracks >5 mm and a select set of tracks between 3-5 mm long; tracks <3 mm were not measured. The obvious point of this plot relates to the enormous scatter of data points if all tracks were plotted. Obviously, any reported data scatter (e.g., Burchell and Thomson, 1996) strongly depends on the somewhat arbitrary and highly interpretative selection of a cut-off value for short tracks. Also note that the longest tracks in the 3.4 and 5.3 km/s experiments seem to be short relative to the general trends in the data, especially those at neighboring velocities. It is such experiments that we would reject in their entirety as unsuitable due to possible projectile fragmentation. Also note that the longest tracks in Figure 9a define some general, qualitative trend of increasing track length with decreasing velocity. However, we do not have enough confidence in the data to justify further quantification. We are simply not certain about the actual impactor mass responsible for these track populations.

The latter point is further emphasized in Figure 9b, which plots track length against the diameter of the projectile residue (D_r). The latter was measured in situ, via a binocular microscope, and is normalized to the nominal 50-μm-diameter projectile (D_p); the precision of the D_r measurements is low, about ±20% for large (>30 μm) residues and ±50% for smaller fragments. While this plot shows that there is some gross correlation of track length and relative residue size, it also shows that individual tracks cannot be interpreted with confidence in an internally consistent manner. Grossly similar residues (e.g., at $D_r/D_p = 0.5$) may be found at the termini of tracks that differ vastly in length. This poor correlation may reflect, in part, a significant spectrum of impact velocities among severely fragmented projectiles, and/or may result from additional projectile fragmentation and track splitting during penetration. On average, the high-velocity experiments tend to produce the smaller residues, which, in turn, represents further evidence for progressively severe projectile breakup as impact velocity and associated accelerations increase.

For the time being we are forced to select, in some defensible and prudent fashion, a population of tracks (Figures 6 and 7) or residue sizes (Figure 10) that best represent specific initial impact conditions. Figure 10 summarizes the relative residue size as a function of aerogel density for all 50-μm projectiles at a constant impact velocity of 6 km/s. As was the case in Figures 6 and 7, we plotted all data points for the Al and glass shots, but only select data for the Allende and Pampa-A powders reflecting only the largest residues. Clearly, all projectile materials have undergone some mass loss, yet one may recover substantial residues (>50% of the projectile's initial size) at 6 km/s using 0.02 g/cm^3 aerogel collectors. Under all conditions simulated, aluminum suffers the least mass loss, and soda-lime glass is superior to the powdered meteorites. At face

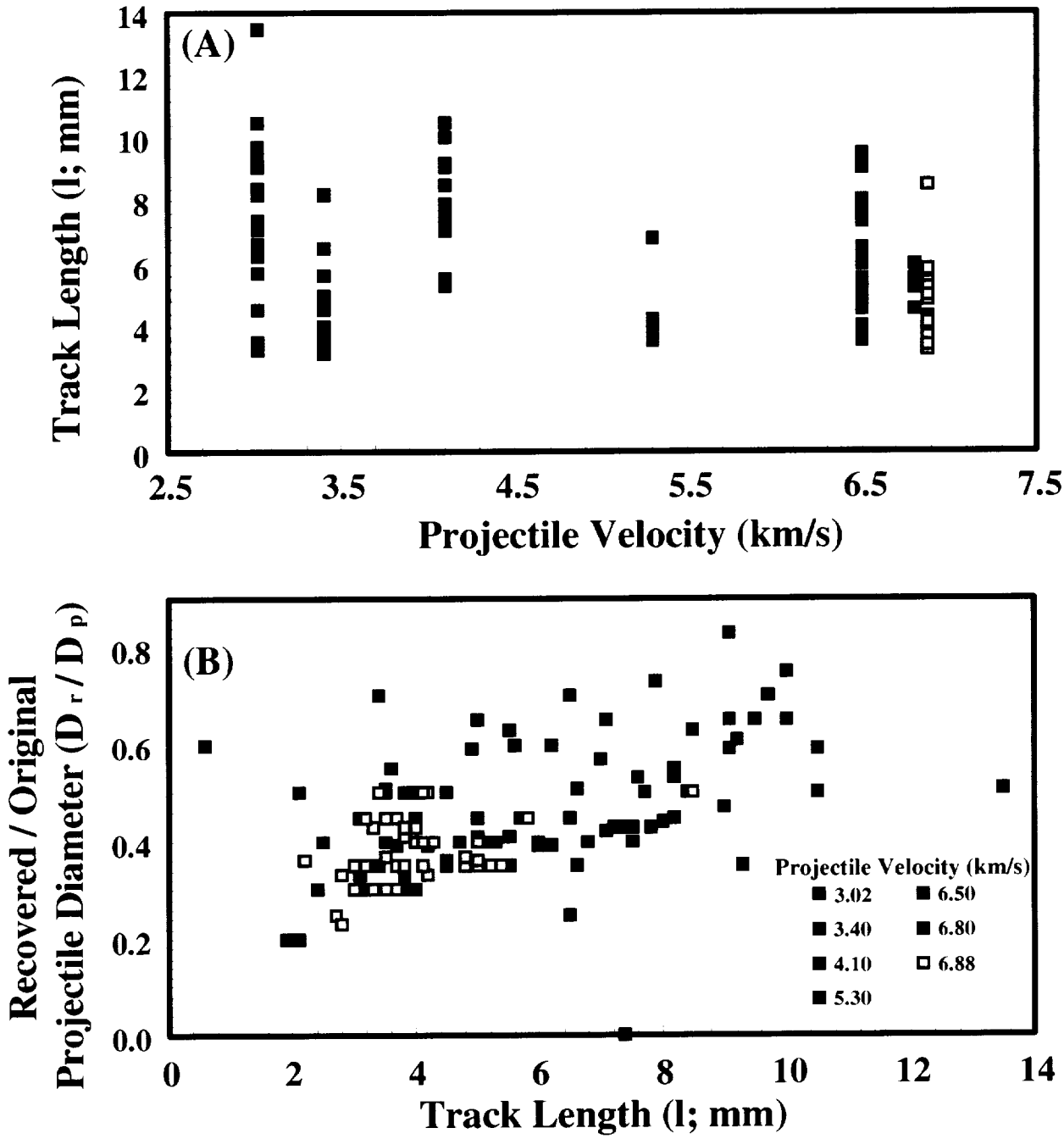

Figure 9a-b. Evidence of projectile fragmentation during launch in the light-gas gun. (a) Variation of track length in individual 0.02-g/cm^3 aerogel experiments by 50-μm Allende projectiles. The apparent cut-off of tracks under 3 mm in length is arbitrary; the plot does not portray the correct frequency distribution of tracks 3-5 mm in length. The longest tracks in each experiment were measured and suggest some inverse dependence of impact velocity and track length. The 3.4-km/s and 5.3-km/s experiments are believed to illustrate severe projectile breakup, in that no large projectile reached the target. (b) Absolute track length plotted as a function of the diameter of the recovered residues (D_r) normalized to projectile size (D_p, 50 μm) for the same experiments depicted in (a). There is a general positive correlation between D_r and l, yet the data scatter is so substantial that quantitative information cannot be extracted with confidence.

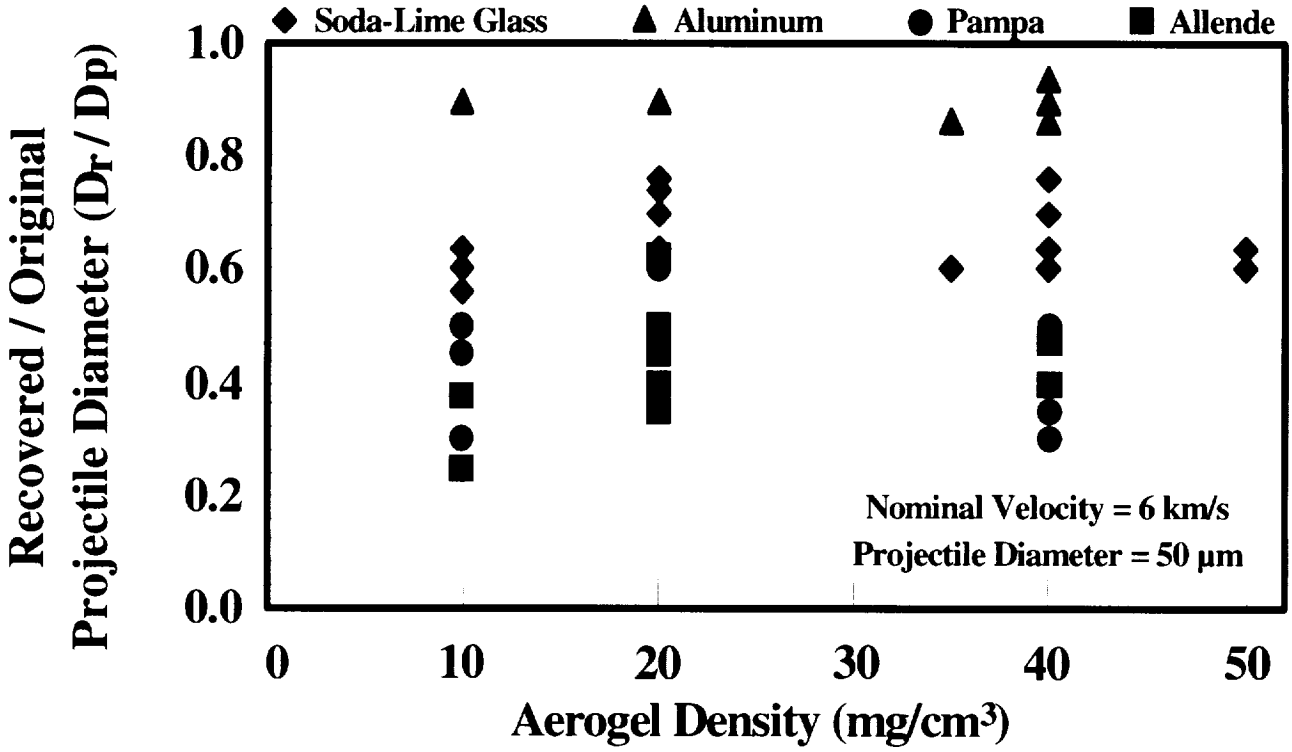

Figure 10. Summary of recovered residues sizes for good (see text) tracks associated with soda-lime glass, aluminum spheres, Allende, and Pampa-A projectiles, all of which were 50 μm in diameter and impacted at a velocity of 6 km/s. All projectile types experienced some mass loss during aerogel capture, with aluminum being preserved the best, followed by glass. Note that the Allende and Pampa-A data are afflicted with substantial uncertainties regarding the exact pre-impact size of the projectile.

value, recovery of all silicates seems to be best at aerogel densities between 0.02 and 0.04 g/cm^3; aerogels of higher and lower density seem to exhibit inferior recovery properties, but this suggestion must be verified by additional experiments. In general, the recovery efficiencies illustrated in Figure 10 are approximately a factor of two higher than those found for 80-μm glass spheres encountering higher density aerogel (0.09 g/cm^3, Thomson, 1995; Burchell and Thomson, 1996).

Figure 11 shows typical large residues recovered from the present experiments. Detailed mineralogical/ geochemical investigations are presently being conducted to determine potential modifications of the particles' phases and textures during the capture process. It is clear that substantial mass loss occurs and that irregular particles will be substantially rounded during aerogel penetration. Note also that molten aerogel adheres to the surfaces of the residues and may even invade the latter along microcracks as detailed by Barrett et al. (1992) or Mendez (1995). Typically, the front faces of the recovered projectiles are associated with massive plugs of compressed and molten aerogel. Such plugs may play a role in the deceleration process by providing some cushioning effect for the projectile.

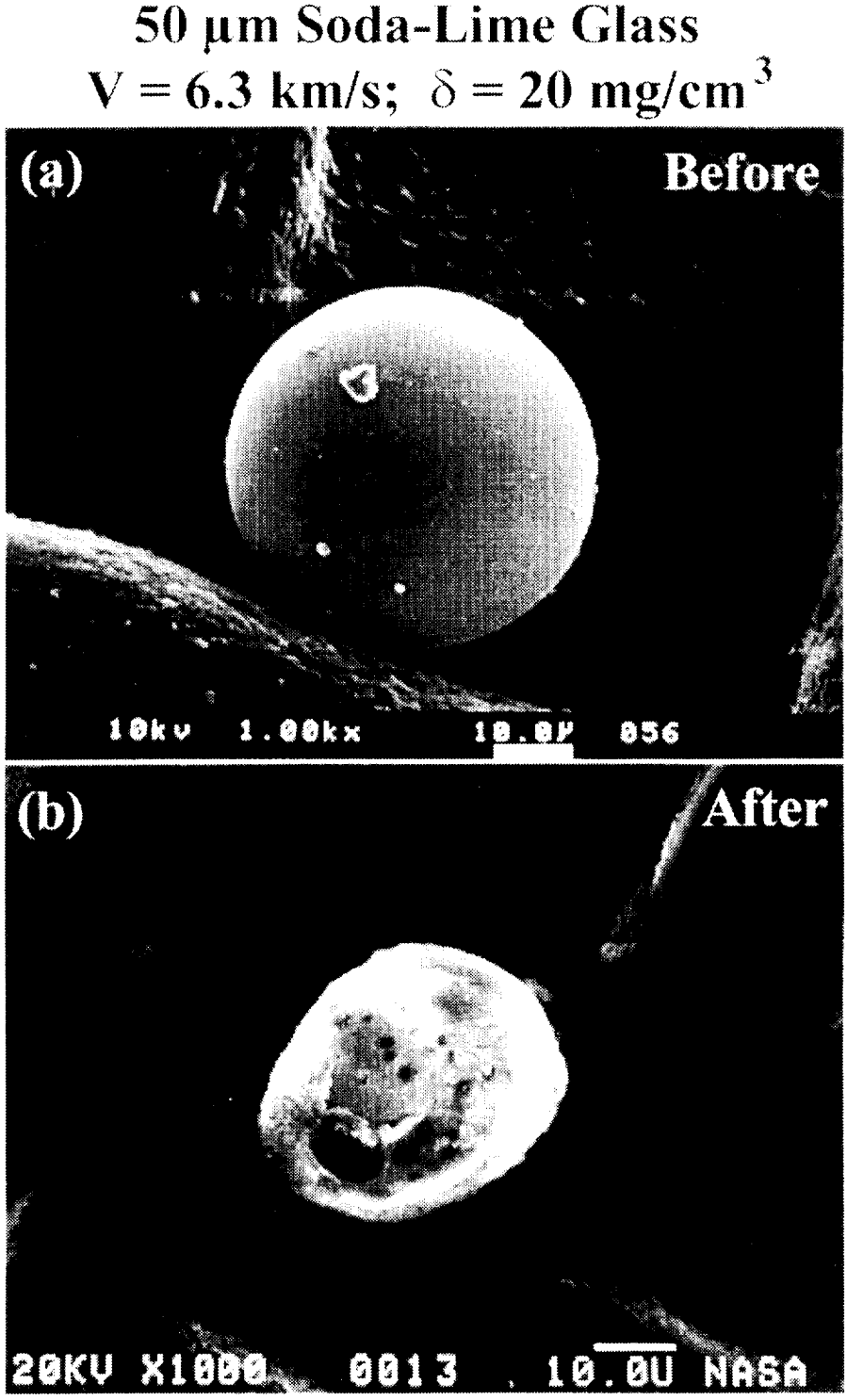

Figure 11a. SEM photographs of typical, largest residues collected at 6 km/s using 0.02-g/cm^3 aerogel. These particles have not been otherwise characterized for possible modifications of texture, phase, or bulk composition. (a) Soda-lime glass sphere, (b) Allende particle, and (c) Pampa-A particle. Note that the meteorite particles compared to those shown in Figure 2 are substantially rounded, and that all residues are partly draped by molten aerogel.

50μm Allende grain into AEROGEL

@ 6.0 kilometers per second

AEROGEL Density = 20mg/cc

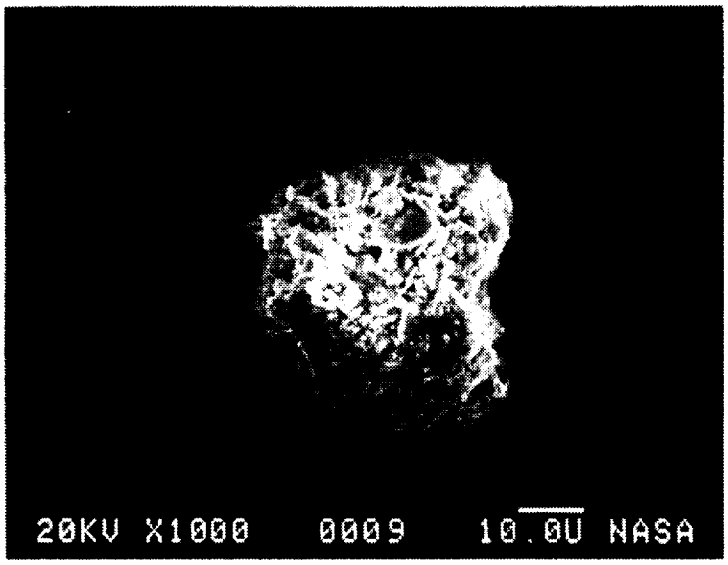

SEM image of pre-shot grain of Allende meteorite projectile.

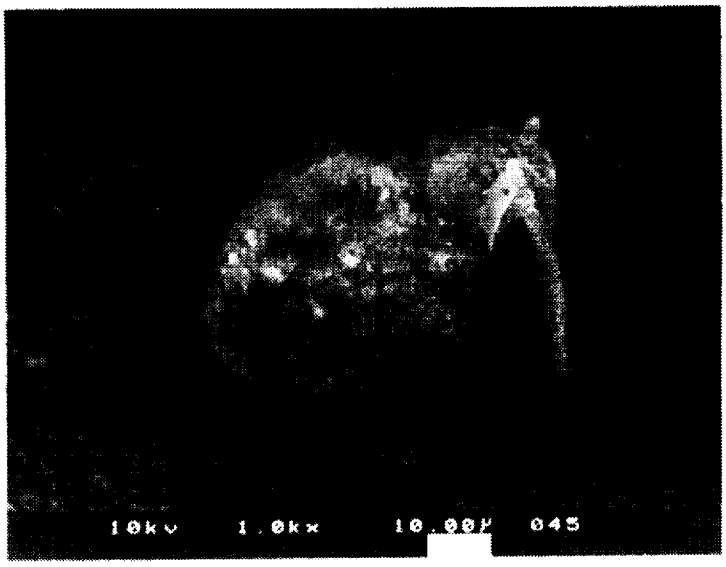

SEM image of Allende projectile recovered from a penetration track into a 20mg/cc AEROGEL target.

Figure 11b. SEM photographs of Allende particle residues collected at 6 km/s.

50µm Pampa grain into AEROGEL

@ 6.0 kilometers per second

AEROGEL Density = 20mg/cc

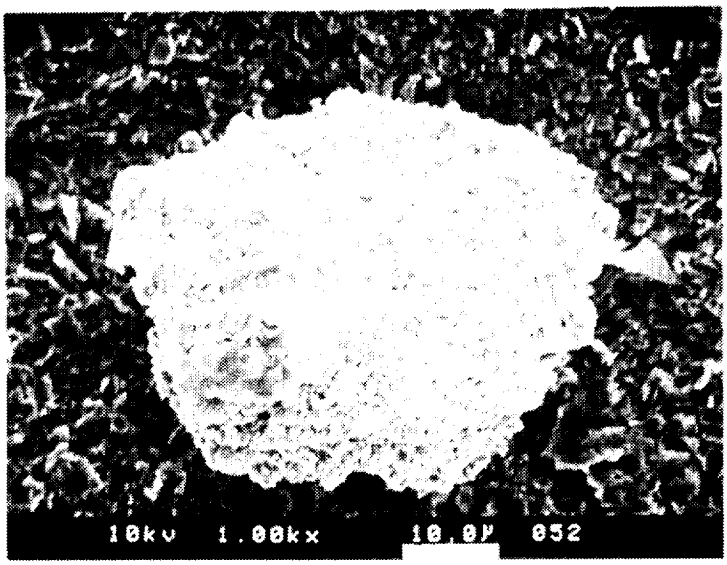

SEM image of pre-shot grain of Pampa meteorite projectile.

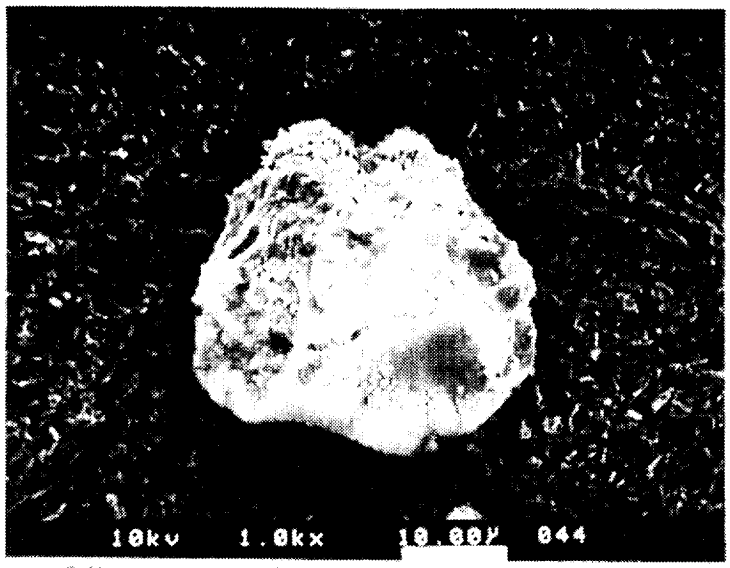

SEM image of Pampa projectile recovered from a penetration track into a 20mg/cc AEROGEL target .

Figure 11c. SEM photographs of Pampa-A particle residues collected at 6 km/s.

Summarizing this series of experiments that mainly addressed the effects of aerogel density, impact velocity, and projectile physical properties, we found that the length of penetration tracks strongly depends on aerogel density and, in complex ways, on impact velocity and projectile properties. The data currently in hand do not allow much more detailed conclusions, as they are afflicted with substantial experimental uncertainties regarding exact initial impact parameters, most notably projectile size. Calibration experiments with very small impactors turned out to be unexpectedly challenging when employing light-gas guns and associated shot-gunning methods to accelerate an aggregate of multiple projectiles. Clearly, the subjective differentiation into good or bad penetration tracks, as practiced in this work, is an unsatisfactory procedure. The substantial scatter of results reported by Thomson (1995) and Burchell and Thomson (1996) are most likely due to similar experimental uncertainties, as was the case in our previous experiments as reported by Barrett et al. (1992). On the other hand, the present experiments employing unbroken, spherical projectiles (e.g., Figure 6 or 7) demonstrate that track length and other experimental effects may be reproduced with good precision. Clearly, initial projectile mass and shape must be better controlled and reproduced than we were able to accomplish in this study. This is a substantial challenge in itself considering the small size (<100 μm) and the large numbers (50 to 100 per experiment) of projectiles needed for systematic studies, that must also include a variety of projectile materials.

5. Experiments at Oblique Impact Angles

The aerogel collectors exposed on the *Mir* station intercepted natural and man-made particles at essentially unconstrained impact angles of 0° to 90° from the target surface at encounter velocities of ~10 km/s for man-made debris and approaching 20 km/s for natural dust particles (e.g., Zook, 1993). In contrast, the *Stardust* collectors will be pointed normal relative to freshly released particles from Comet Wild 2, while the encounter velocity is expected to be a modest 6.2 km/s based on current mission profiles. Interpretation of the *Mir* collectors demands that the relationships of penetration track length, impact velocity, and impact angle be known. In addition, Tsou (1990) suggested that inclination angle and absolute track length could be used to reconstruct the trajectory of individual particles.

Based on these considerations, the objective of our second test series was to evaluate track length as a function of impact angle and velocity. A single projectile type (soda-lime glass) was used, as well as a constant aerogel density (0.02 g/cm^3). These tests employed the so-called "slabbed" target configuration (Fig. 1c), since the initial tiles (Shipment II) were too thin (10 to 12 mm) to accommodate the expected track lengths. Wedges of 60°, 45°, and 30° were attached to the target-support plate, onto which the entire target assembly is mounted. In addition, we began to suspect that aerogel density may vary among Shipment II samples. Therefore, we exposed the same aerogel specimen to multiple gun-firings (≤4 times), with each exposure typically occurring at a different impact angle. The inclination of individual tracks relative to the target surface is sufficiently distinct (Fig. 12) to permit assignment of individual tracks to any specific experiment at some given impact angle. We also repeatedly exposed individual targets at constant impact angle with variable impact velocities; in this case, all tracks (typically fewer than five) were measured for length and their X-Y positions were marked on the cardboard hold-down frame before the next experiment, each experiment using different-colored pens.

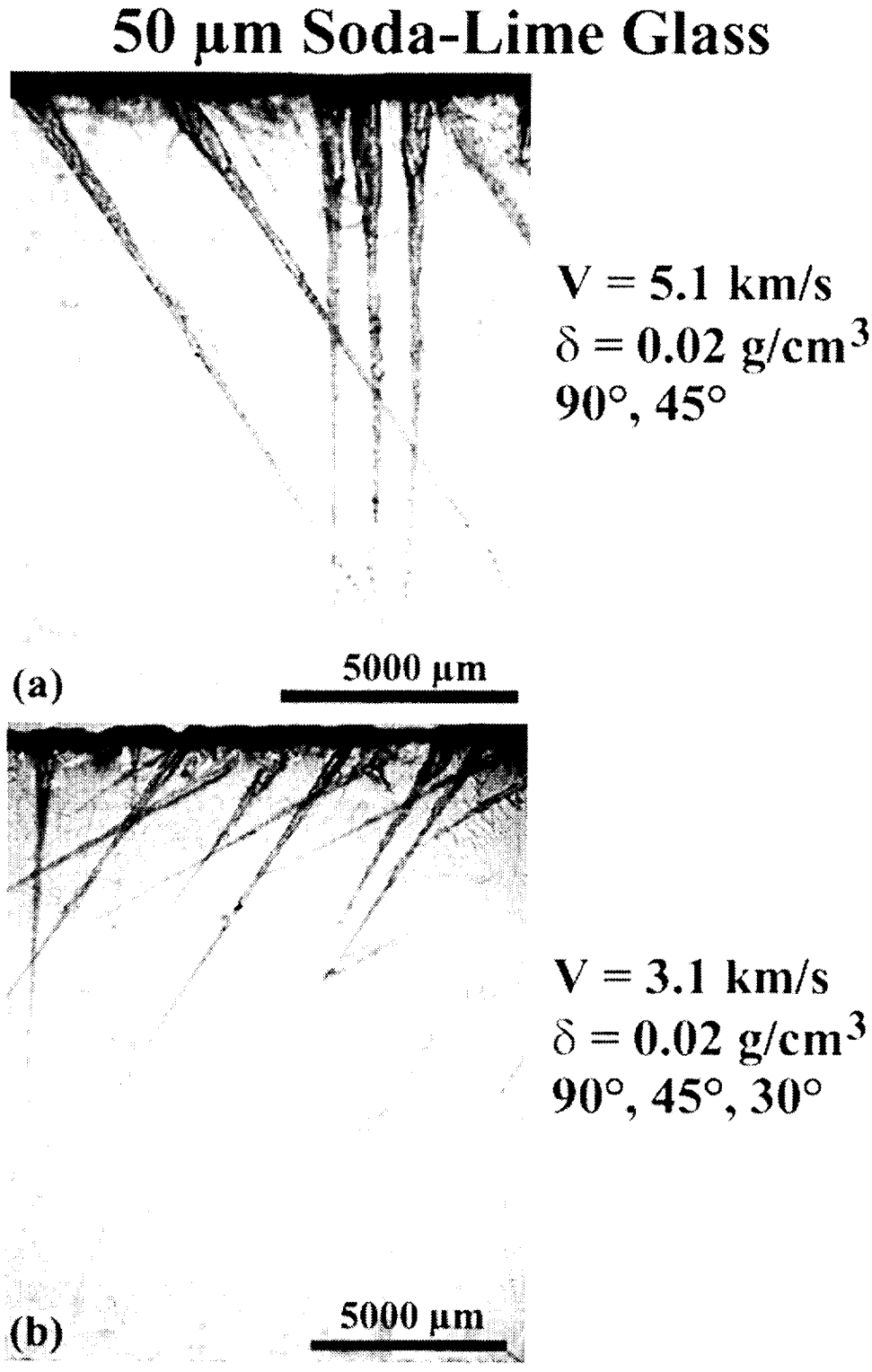

Figure 12a-b. Examples of aerogel penetration tracks produced at variable impact angles. Target (a) was exposed twice, while target (b) was used in three experiments, as can be seen from the variable inclinations of the penetration tracks. Note the overall reproducibility of track length among individual and different experiments in any given aerogel specimen.

The need for multiple exposure of the same aerogel specimen to ensure constant target density was determined during some normal incidence experiments using Shipment II targets that did not reproduce the (glass) data illustrated in Figures 8 and 9. Some tracks were shorter than those produced earlier, and we suspected variable target density to be the cause. Examples of such track variations from tile-to-tile are illustrated in Figure 13, which shows track lengths in a single (Shipment II) target at 90° and 45°, and a repeat test at 45° into a second (Shipment II) aerogel sample; both targets possessed a nominal density of 0.02 g/cm^3. Note the substantial overlap of experiments 1864 and 1865, and the difference with duplicate experiment 1866. Also note the good agreement of shots 1864 and 1865 with equivalent experiments in Shipment I tiles (Figure 7), all yielding tracks ~12-14 mm long. Clearly, experiment 1866 systematically yielded shorter tracks and we suspect that target density was higher than the nominal 0.02 g/cm^3. In detail, tracks within a given aerogel tile that are either on the short or long side are often juxtaposed, possibly indicating density variations within a specific specimen, but the present data are insufficient to conclusively demonstrate such intra-tile variations.

Figure 12 illustrates representative results of the oblique-impact tests . Note the paucity of short tracks considering that the targets were exposed to multiple gun-firings (i.e., twice [Fig. 12a at 90° and 45°] and three times [Fig. 12b at 90°, 45°, and 30°], respectively). Figure 12a is somewhat unusual and illustrates three vertical tracks of identical depth and two inclined tracks, also of essentially identical length; the projectile mass/energy and target density seem exceptionally constant, yielding such reproducible results (Figure 12a). Figure 12b is more typical of the present aerogel experiments and does exhibit noticeable scatter in track length for any specific angle of incidence, presumably associated with impactors of variable mass. In most cases, the reproducibility of track length in similar experiments is not as good for the Shipment II tiles as it was for the experiments that employed Shipment I aerogel tiles (Figure 6 and 7).

Returning to the major objective of this second series of experiments, Figure 14 summarizes all observations of track length as a function of impact angle and velocity for 0.02 g/cm^3 aerogel and 50-μm spherical soda-lime glass projectiles. Figures 14a-14d illustrate track lengths at nominal velocities of 3, 4, 5, and 6 km/s, respectively, while Figure 15 shows averaged data for easy comparison. In general, the data are disappointingly and surprisingly uniform, as there is not a clear relationship of track length with impact angle or velocity. The 6.2-km/s, 60° impact-angle experiment appears to be a particularly uncooperative dataset that we are at a loss to explain.

Nevertheless, what is apparent from Figures 14 and 15 is that all tracks have similar lengths and other morphologic attributes regardless of impact angle. The total mass displaced and damaged by oblique impacts appears to be insensitive to impact angle, unlike cratering events in dense media that predominantly reflect only the vertical velocity component (e.g., Christiansen et al., 1993). We interpret the data in Figures 14 and 15 to imply that processes other than pure shock phenomena play the dominant role in the penetration of low-density, porous media, an observation in support of the continuum mechanics model of Anderson and Ahrens (1994). This model largely relies on a bulk-viscosity term, drag forces, and ablative processes for the deceleration of hypervelocity impactors in porous media of exceptionally low bulk-density.

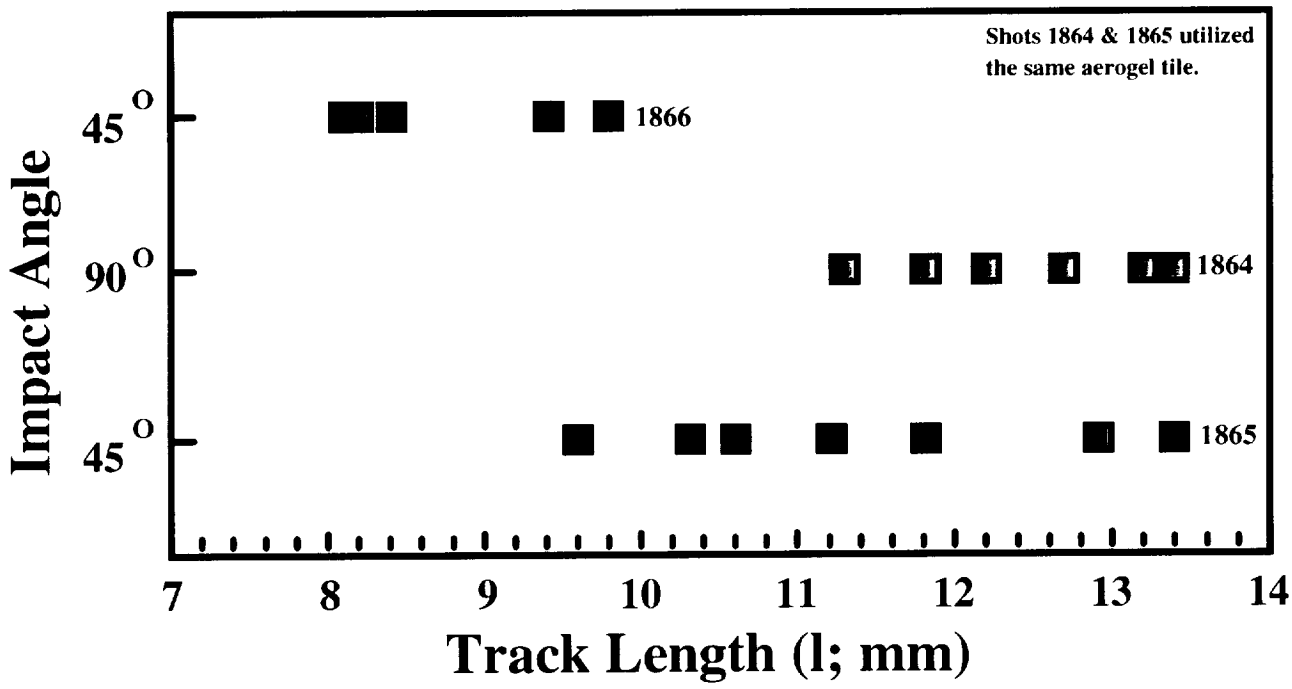

Figure 13. Plot of track length versus impact angle showing the reproducibility of track lengths per experiment using 50-μm aluminum spheres and 0.02-g/cm^3 aerogel at impact angles of 90° and 45°. Individual aerogel tiles were utilized in multiple experiments; shots 1864 (V = 5.03 km/s) and 1865 (V = 5.13 km/s) used the same tile, while a second slab was used for experiment 1866 at V = 4.98 km/s. Note that the tracks in 1866 are systematically shallower than those of 1865, which is essentially a duplicate experiment (see text).

The experiments at inclined impact angles corroborate the findings of Tsou (1990) and Thomson (1995) who found that the track orientation faithfully records an initial impact angle. Our data, however, do not support the suggestion by Tsou (1990) that complete trajectory data (i.e., direction and *velocity*) may be extracted from the inclination and length of penetration tracks in low-density foams. In an earlier work (Hörz et al, 1992), we disagreed with this view and continue to maintain that the encounter velocity is not readily obtained from absolute track length, a conclusion also reached by Thomson (1995), and Burchell and Thomson (1996).

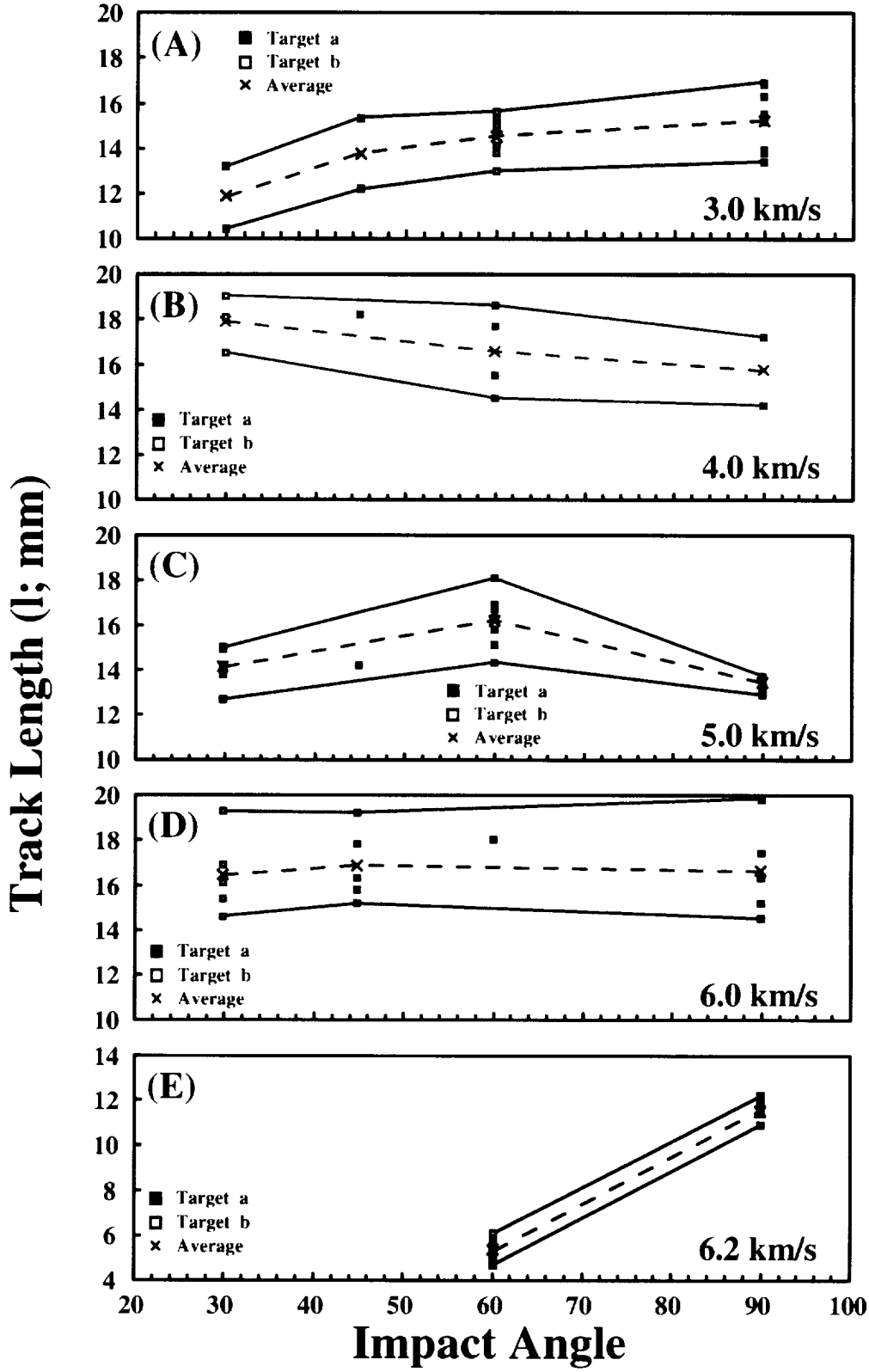

Figure 14a-e. Track length as a function of impact velocity and impact angle for 50-mm soda-lime glass spheres and 0.02-g/cm^3 aerogel. The solid lines connect the shortest and longest track per experiment, while the dashed line represents the average of all tracks for a given set of impact conditions. The 6.2-km/s experiments appear to be anomalous; all tracks at 90° occurred in one aerogel tile, while those at 60° occurred in another; the latter tile was reimpacted at 60° and the short tracks were confirmed; we suspect that this specific tile possessed a higher density than the nominal value of 0.02 g/cm^3.

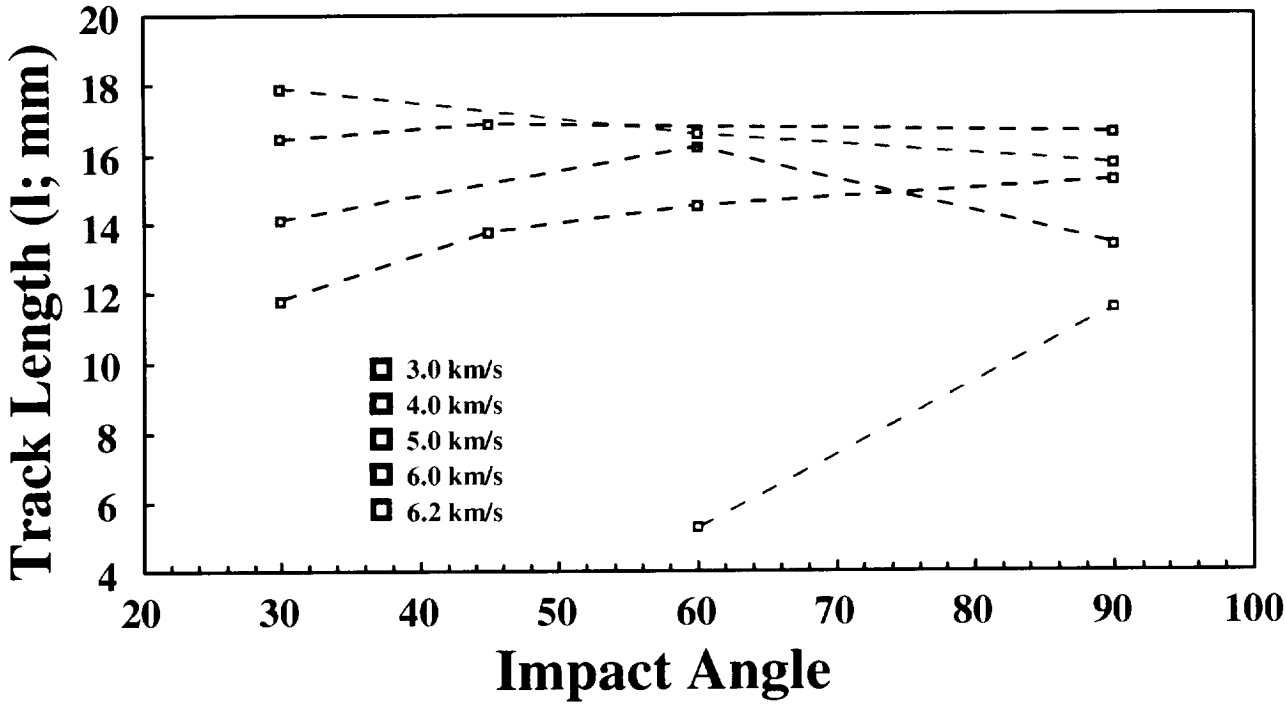

Figure 15. Summary plot of the average track lengths, depicted in Figure 14, as a function of impact angle and velocity. Note the fairly constant track length at most impact angles, as well as at any given velocity. These represent the best calibration data we currently have, as they were generated with unbroken soda-lime glass spheres (see text).

6. Experiments With Particles of Low Cohesion

Particles of low-cohesive strength, typically with low density and some porosity, constitute an important subclass of natural cosmic-dust particles (e.g., Love et al., 1993). Because their physical properties substantially differ from those of dense silicates and rock, their cratering and penetration behavior may not readily be extrapolated from impact experiments using dense, non-porous projectiles. As a consequence, dedicated impact simulations are required to delineate the penetration behavior and capture efficiency of porous materials of low-cohesive strength. However, hypervelocity accelerators, including light-gas guns, cannot readily launch materials of low-cohesive strength. The following section describes two new approaches that produced impactors of low-cohesive strength traveling at 6 km/s; although such impactors may not be well characterized, they will be helpful in answering some first-order questions about penetration and retention of "fluffy" cosmic-dust particles in aerogel.

6.1 Cocoa Powder

A number of fine-grained (<1 μm), flour-like materials were mixed with nominal projectiles in an attempt to eliminate projectile fragmentation during light-gas gun acceleration. The idea was to provide some cushioning between neighboring projectiles inside the sabot cavity. None of these tests resulted in a noticeable improvement of unbroken, nominal projectiles. Somewhat fortuitously, however, our tests with commercial cocoa powder resulted in various clumps of the powder impinging upon the aerogel target. Such clumps made crater-like tracks on dimensional scales of a few millimeters. Unfortunately, we had no control on the

clump size, so variable track sizes resulted. The velocity detectors at the target site ($t_{1\text{-}n}$) measured arrival times of the early clumps at a velocity identical to that of the sabot impact(s) and consistent with expected projectile velocity, based on empirical gun parameters. However, there was an extra long tail to the arrival times of the impactors, with some events occurring as late as 300 μs after the first signals, corresponding to a decrease in impact velocity of around 20%. It follows that projectile velocity is essentially uncontrolled for these tests; the values given are those for the first arrivals.

Figure 16 illustrates representative examples from experiments that employed a 1:1 (weight) mixture of cocoa and 50-μm aluminum projectiles. The presence of cocoa clumps is readily apparent from the characteristically stubby nature of some tracks that are distinctly light brown in color. Figure 16a illustrates two experiments, one at 90°, the other at 45°, while Figure 16b shows only one experiment at 90°. Note the stubby nature of the tracks, none resembling their slender counterparts seen in Figure 4. Frequently, a relatively slender, long track emerges from the stubby and bulbous cavities as detailed in Figures 16c and 16d, containing nominal aluminum-projectile residue at their termini. Such tracks were absent in a control shot that launched only cocoa powder. This suggests that the compound tracks visible in Figure 16 are the result of nominal impactors that had variable amounts of cocoa powder clinging to the projectile. While long compared to the pure cocoa-powder control shot, such composite tracks are substantially shorter than those associated with pristine aluminum spheres (e.g., Figure 6a). Unfortunately, tracks without evidence of some cocoa powder adhering to the projectile were absent. Therefore, the idea of cushioning the nominal projectiles by some fine-grained powder was abandoned as it did not yield impactors of well-controlled mass. Nevertheless, the cocoa experiments relate to the penetration of aerogel by low-density, porous, weakly cohesive particles.

Figure 16e shows the interior of a track produced by impact of one of these cocoa-powder clumps; the aerogel target was sectioned via a razor blade. Much of the dark material adhering to the walls is brown, remnant cocoa powder. Figure 17 shows detailed SEM studies of a single cocoa track produced at 6 km/s. Figure 17a reflects standard optical photography of the unprocessed, pristine track at some modest depth inside the (1-cm-thick) aerogel slab. In contrast, the SEM image of Figure 17b was taken after careful splitting of the slab and presents a detailed view of the track interior. Comparison of Figure 17a and 17b indicates that additional breakage and damage in the vicinity of the track occurred during splitting of the aerogel via the razor blade method. The track interior is substantially blocky and, surprisingly, there is no evidence of abrasion or fine-scale erosion. Figure 17c shows the entrance hole for the track, taken prior to splitting, and its irregular outline suggests an irregular cross-section of the impactor. Some radial cracks exist, as well as poorly developed concentric fractures, none of them sufficient to initiate spallation of the aerogel surface. Figures 17d and 17e illustrate progressively higher magnifications of the pristine track interior, viewed through the entrance hole. Again, the largely blocky nature of the track walls is evident, yet some areas seem to be crushed more intensely than others (e.g., lower right-hand corner in Figure 17e). As before, there is no evidence of striation or of melting phenomena. Abundant, fine-grained debris populates the freshly created, brown surfaces. Some of this fine debris, and an occasionally larger particle, such as the pear-shaped object in the lower left-hand corner of Figure 17e, display prominent charging effects and are interpreted as remnants of cocoa powder. These cocoa residues are the objects of ongoing chemical analyses.

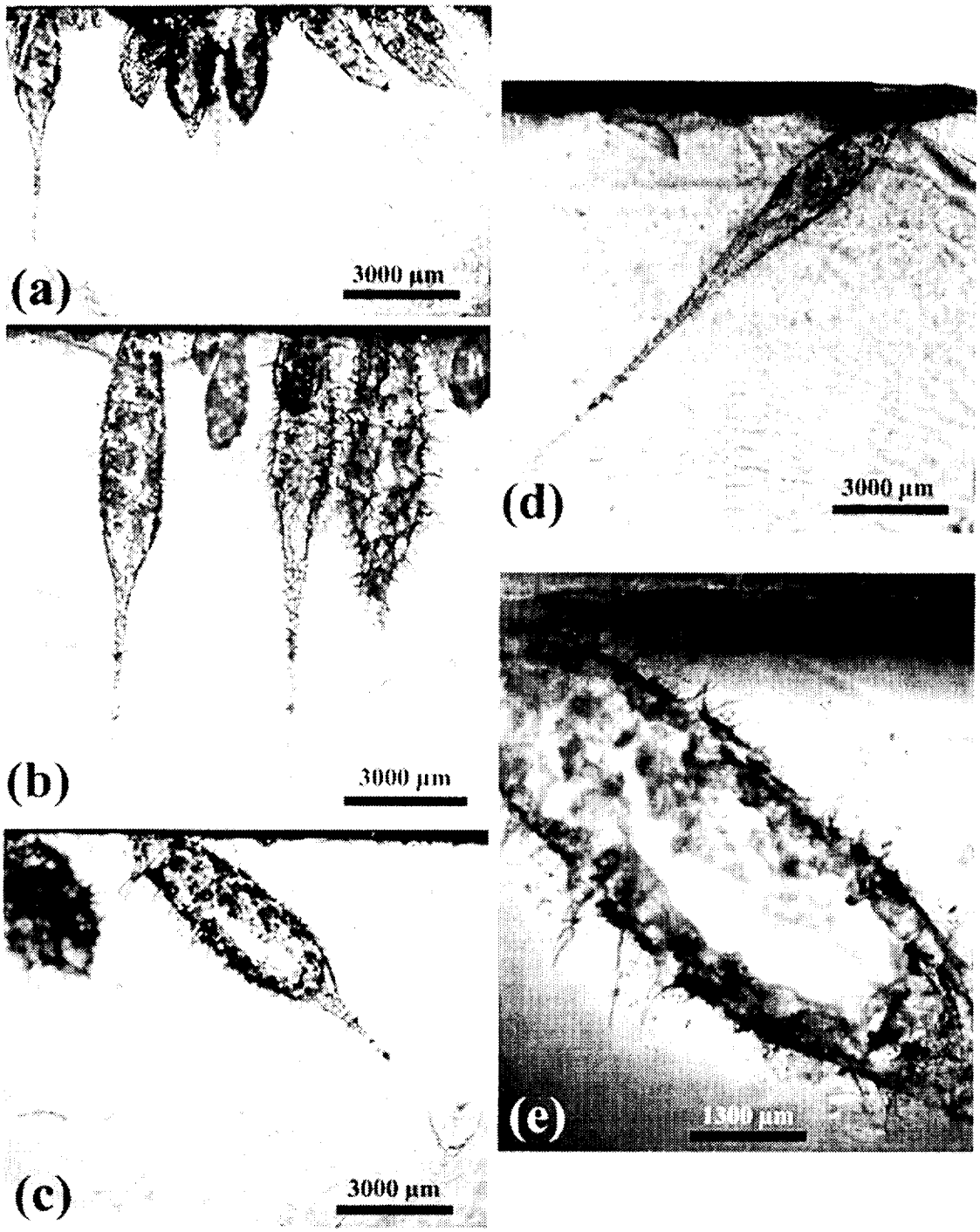

Figure 16a-e. Optical photographs of penetration features in 0.02-g/cm³ aerogel produced by a 1:1 (weight) mixture of cocoa powder and 50-μm aluminum spheres. (a) Typical tracks resulting at 5.1 km/s and impact angles of 90° and 45°, respectively. (b) Additional tracks from the 90° at 5.1 km/s experiment of (a). Note the bulbous, stubby nature of the short tracks by pure-cocoa clumps, as opposed to the longer, composite tracks resulting from nominal aluminum projectiles embedded into a cocoa matrix or that had substantial clumps of cocoa adhereing to their surfaces. Figures (c) and (d) show typical 45° impacts at 6.0 and 4.7 km/s, respectively, suggesting different amounts of cocoa associated with the aluminum spheres. (e) Enlarged view of the track in (c).

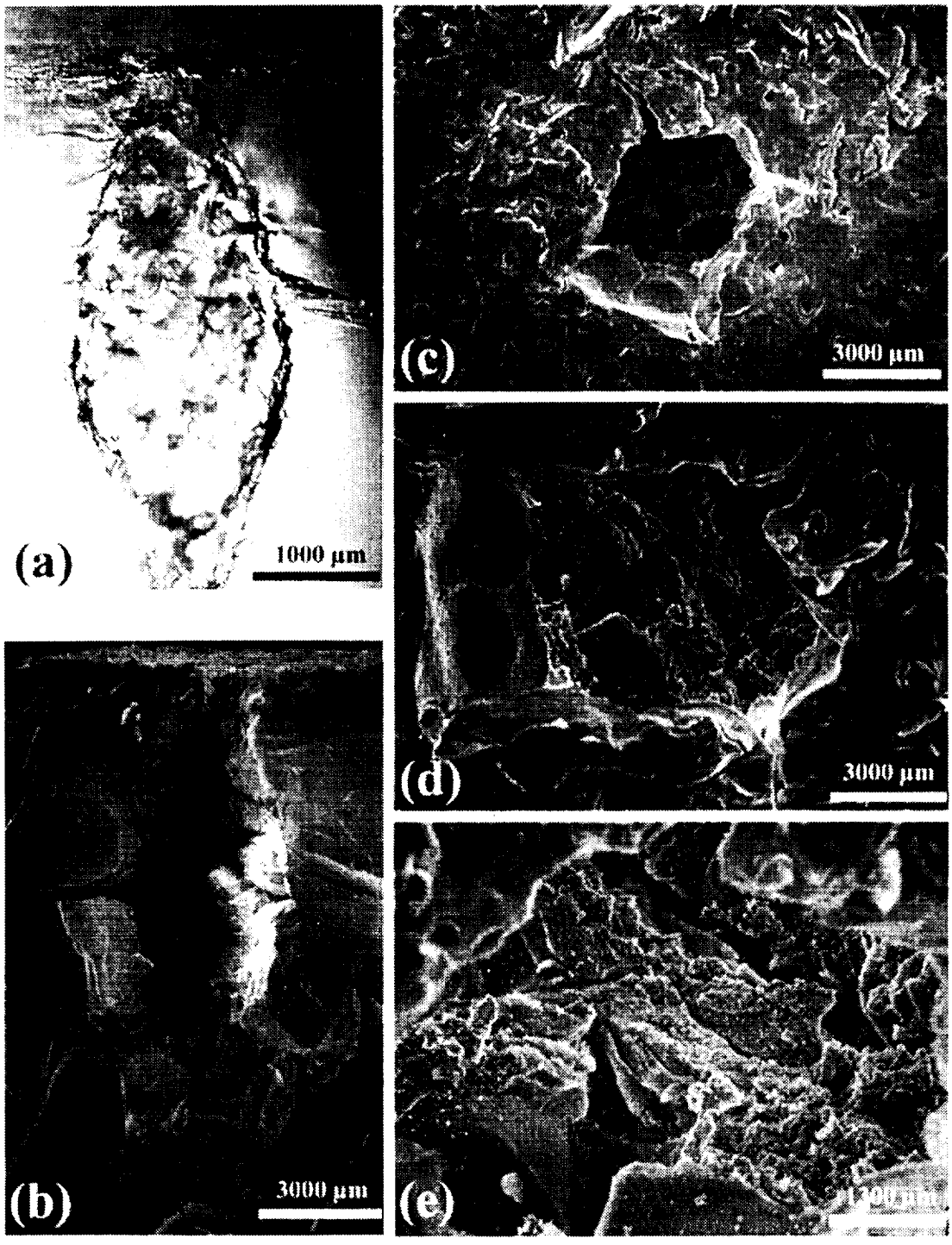

Figure 17a-e. Detailed views of a cocoa track produced at 6 km/s and 90°. (a) Optical image of entire track, (b) detailed track interior, (c, d, e) various enlargements of the track entrance hole and interior. Most of the fine particles are cocoa powder (see text).

These experiments with cocoa clods are interesting from a phenomenology point of view, because individual clods may be viewed as analogs of the physical properties of fairly friable, fluffy, and porous natural particles. These impact tests are significant as they demonstrate, for the first time, that residues of such poorly cohesive, and generally low-density aggregates may be successfully trapped in aerogel collectors at velocities as high as 6 km/s. The composite, long tracks produced by cocoa-coated, nominal impactors suggest that relatively large and dense components of natural aggregate particles may also penetrate in differential fashion relative to the fluffy matrix, making deep, subsidiary tracks that emanate from otherwise stubby and bulbous aerogel cavities. In addition, there is considerable interest in the exobiology community regarding the ability of organic compounds to survive impact. If warranted, additional and more detailed experiments could be conducted with fine-grained organic matrices other than cocoa. It seems possible to mix silicates of all sizes (and most likely compositions/structures) with cocoa or other organic materials of more direct interest to exobiology and to evaluate their survivability and/or modification(s) during hypervelocity aerogel capture.

6.2 Clusters of Collisionally Produced Fragments

Our second approach in producing particles of low-cohesive strength is a spin-off from penetration experiments in thin targets, commonly conducted in the development of collisional shields (e.g., Anderson, 1993, 1995). Such experiments typically employ massive witness plates behind a penetrated bumper-foil (e.g., Hörz et al., 1994), or high-speed photography or X-ray shadowgraphs (e.g., Piekutowski, 1993) to monitor the nature and evolution of the resulting debris clouds. Accordingly, fragment-size distribution and radial dispersion angle of the resulting debris plumes depend on bumper thickness and impact velocity for any given projectile. Therefore, it is possible to generate a desired population of fragments from almost any projectile by judicious selection of bumper thickness and impact velocity. In addition, by varying the standoff distance of the witness plate from the penetrated bumper, one may intercept the debris cloud at various stages of radial dispersion; this permits some manipulation of the spatial density of fragments at the location of the witness plate. These considerations were used to expose aerogel, in lieu of witness plates, to clouds of projectile fragments that ranged from barely fractured projectiles to widely dispersed plumes. Obviously, such debris plumes possess no cohesive strength, and they represent conservative end-member conditions in evaluating the capture of fluffy, highly friable, natural particles.

For these experiments, we selected 4-μm-thick aluminum (1100 series) as a bumper foil; this thickness readily disrupts 50-μm soda-lime glass projectiles at velocities above 5.5 km/s and is sufficiently thin to ensure that the debris plumes are totally dominated by projectile debris (Hörz et al., 1994). All experiments in this test series employed aerogel with a nominal density of 0.02 g/cm^3 from Shipments II and III. Standoff distance was varied between 2 and 15 mm from the bumper foil.

We conducted a series of precursor experiments, exposing polished-copper witness-plates, to pin down specific conditions for the aerogel shots. Such solid-Cu plates are not only less costly than aerogel, but they also reflect the size distribution of projectile fragments much better than do the brittle silicate aerogels. This is especially true for tightly clustered fragment clouds that generate many overlapping, yet clearly resolvable craters in copper, but which typically produce only a single, very large entrance hole in the aerogel. Some of

these precursor experiments are shown in Figure 18. Figure 18a illustrates two barely fragmented projectiles at 6.0 km/s and a standoff distance (L) of 4 mm. Note the presence of few very small fragments and the survival of a massive, central core-fragment. Detailed inspection of the interior of the major crater reveals the presence of subsidiary depressions that are separated by ridges and delicate septa, suggesting that this core was an internally fractured object of distinctly heterogeneous mass distribution. Progressive projectile disruption and dispersion as a function of impact velocity is illustrated in Figures 18b and 18c at 6.2 and 6.4 km/s, respectively; L was 2 mm for both shots. Also note the presence of projectile melt, which is manifested by radial (Figure 18a) and increasingly concentric (Figure 18b) stringers and filaments, many of a distinctly beaded nature. As detailed by Gwynn et al. (1996), such features are erosive gouges and depressions of negative relief, rather than depositional features. Figures 18d-18f illustrate the effects of increased standoff distance; note the more widely dispersed fragment impacts. Cumulatively, Figure 18 demonstrates that it is possible to design fragment plumes that range from very tight clusters to widely dispersed clouds by judicious selection of standoff distance and impact velocity. Also note that some debris plumes include a sizable fraction of melt, as evidenced by the highly two-dimensional stringers and beaded filaments that are identical to those from Cu witness-plates as described by Gwynn et al. (1996).

Select experiments that employ aerogel witness-plates are illustrated in Figure 19. Figure 19a and 19b shows features that are essentially equivalents to those in Figure 18a (at 6.03 km/s). All three impact events shown in Figure 19a and 19b are from the same experiment (V = 5.92 km/s and L = 4 mm), and demonstrate the reproducibility of tightly clustered objects using the collisional fragmentation method. Modest dispersal of a dominant, central mass is indicated by the relatively large entrance hole. Figure 19c illustrates increased dispersion of such a mass at L = 15 mm, yet otherwise nearly identical impact conditions (V = 5.94 km/s). Note that some of the large holes visible in Figure 19c (and Figures 19a and b) are complex and compound, suggesting that some of the more massive fragments were themselves internally fragmented, yet not fully disaggregated and dispersed. Figures 20a and 20b present cross-sections of the events illustrate in Figure 19a and 19c, respectively. These cross-sections corroborate the above interpretations of internally fragmented "aggregate" impactors, as numerous small penetration tracks emanate from what may be perceived as a single, major penetration hole (and impacting mass?). These cross-sections enhance the sense of compound impactors, with individual mass elements penetrating differentially. Clearly, variable track lengths mandate a somewhat heterogeneous size distribution among the larger fragments. Note the initially, fairly bulbous penetrations in Figure 20 that are somewhat reminiscent of the previously described cocoa tracks, possibly reflecting a very low bulk density of the impacting mass. Binocular microscope inspection reveals that most of the large tracks exhibit projectile residues at their termini.

The erosive nature of impact by molten projectile materials is detailed in Figure 21, which represents views of one experiment (V = 6.6 km/s, L = 15 mm) at different magnifications. Note the distribution of fine, beaded melt stringers. Most of the melt, however, appears to be concentrated in a horseshoe-shaped loop, most likely the incomplete or distorted equivalent of the ring-shaped melt deposits described by Gwynn et al. (1996). Undoubtedly, the erosive nature of small and large melt particles, including delicate filaments of melt, is obvious in these images. The melts themselves represent low-strength impactors also capable of generating substantial damage and penetration of aerogel targets.

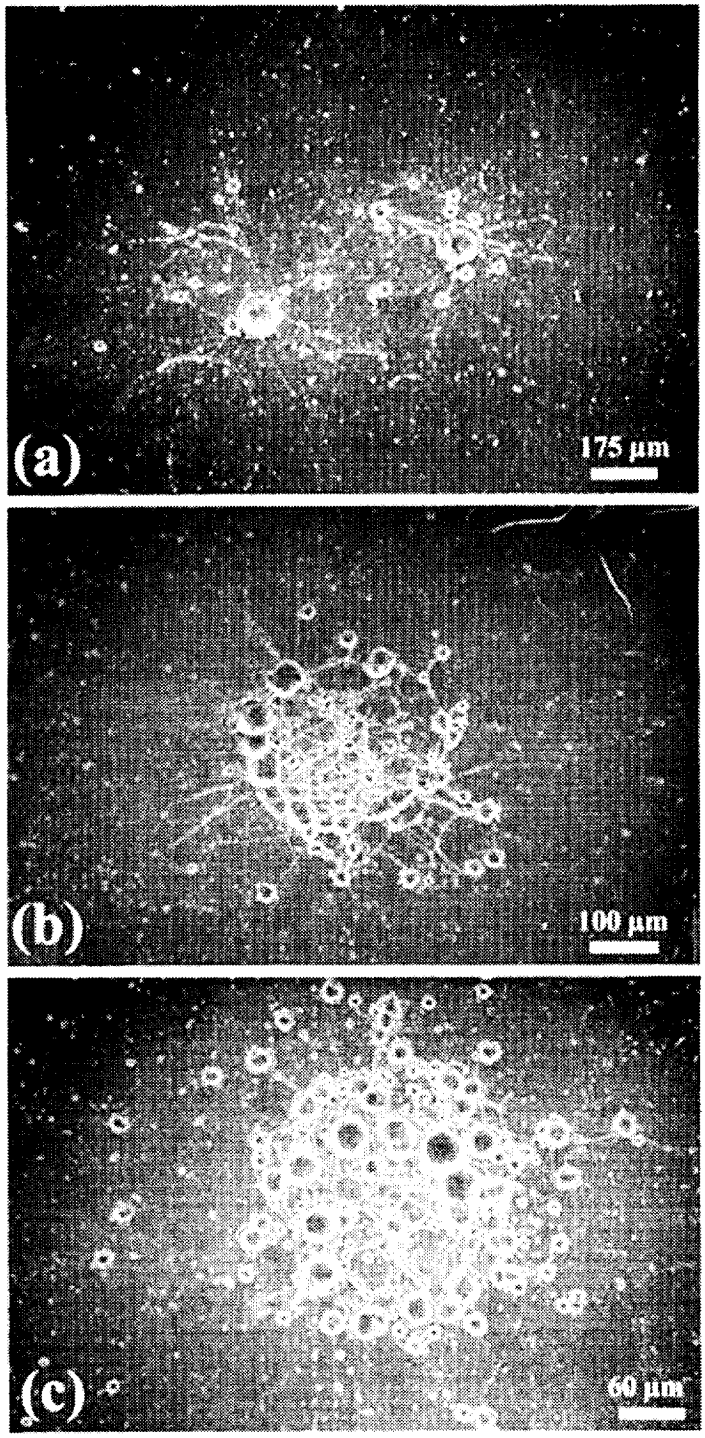

Figure 18a-c. Typical damage patterns on polished copper witness-plates made by a 50-μm soda-lime glass sphere after it was fragmented by passing through a 4-μm-thick Al_{1100} foil. The distance between the foil and witness plate (the standoff distance, (L) is given for each experiment. The images are arranged with increasing velocity. Note that the size distribution of the fragments depends on the impact velocity and that the degree of fragment dispersion can be controlled by varying L. Many of the radial and circular lineaments represent stringers of projectile melt; see the detailed study at larger experimental scales by Gwynn et al. (1996).

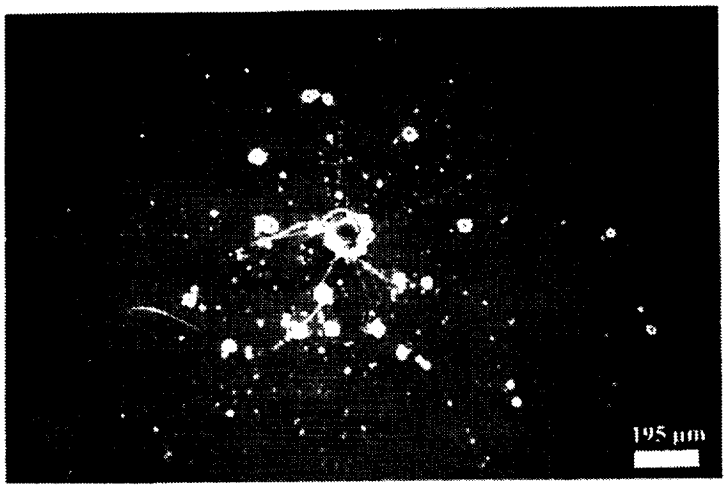

Soda Lime Glass
(50 µm)

Thin-Film: Aluminum
(4 µm)

V = 5.9 km/s
L = 10 mm

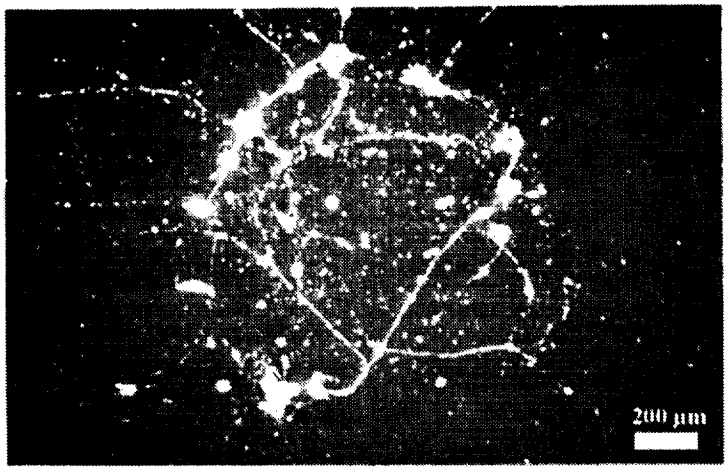

V = 6.2 km/s
L = 10 mm

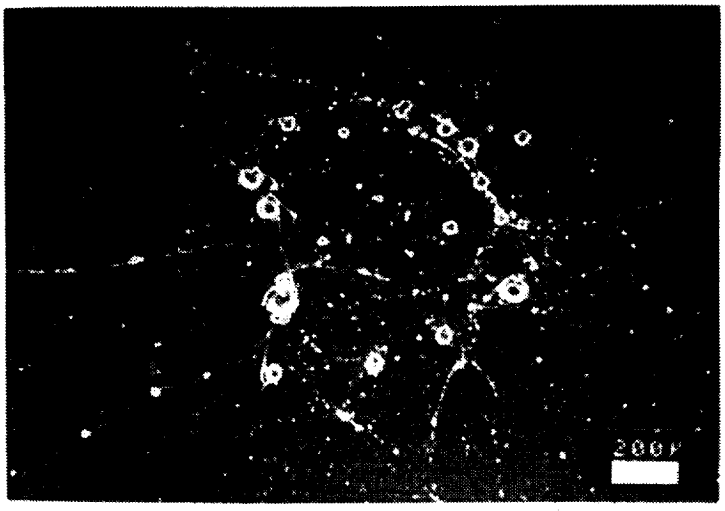

V = 6.7 km/s
L = 10 mm

Figure 18d-f. More widely dispersed fragment impacts due to increased standoff distance.

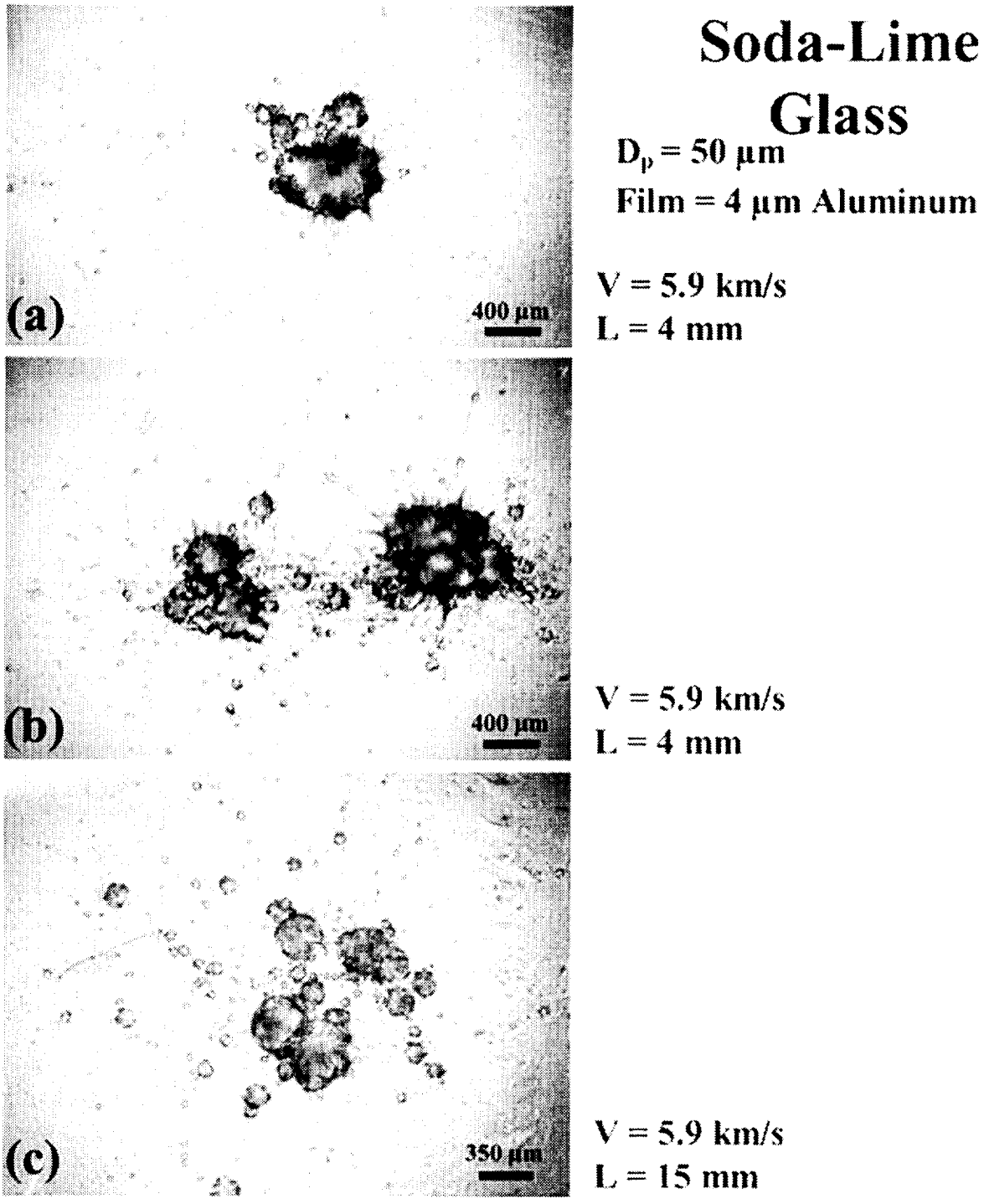

Figure 19a-c. Plan view of impacts into aerogel made by clustered impactors similar to those illustrated in Figure 18, all at about 5.9 km/s. Impacts in (a) and (b) are from the same experiment, illustrating good reproducibility of the fragment clusters; (c) is a duplicate experiment at L = 15 mm, again showing increased geometric dispersion of individual fragments. Note that the tracks are compound features, suggesting the presence of internally disrupted fragment masses that disperse modestly as standoff distance increases (see text).

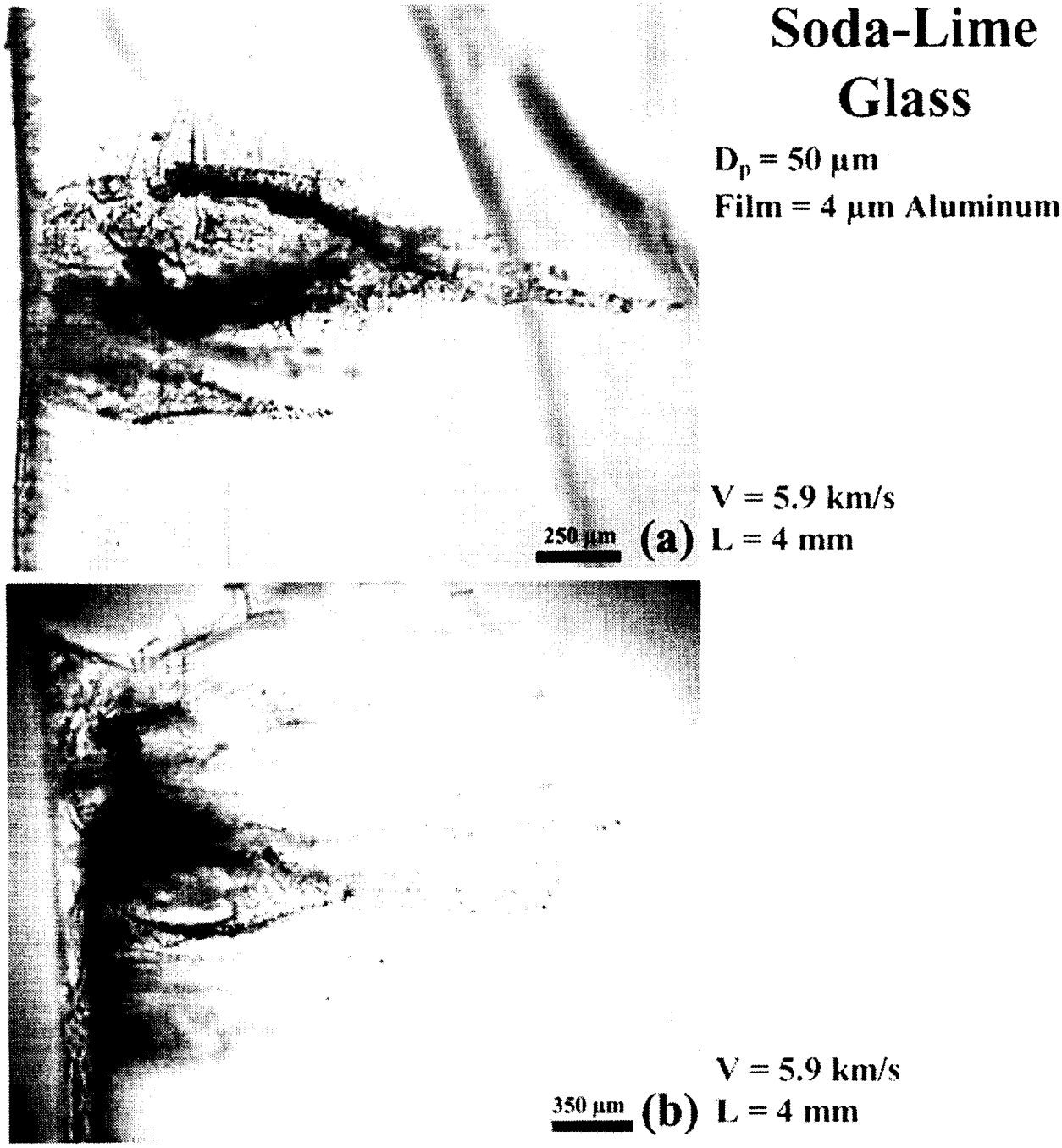

Figure 20a-b. (a) Side views of two compound penetration tracks at 5.9 km/s with a standoff distance of 4 mm, corresponding to Figure 18a; (b) impact velocity of 5.9 km/s and standoff of 15 mm, corresponding to Figure 19c. Note the presence of numerous subsidiary tracks caused by apparently coherent fragments that penetrate deeper (see text).

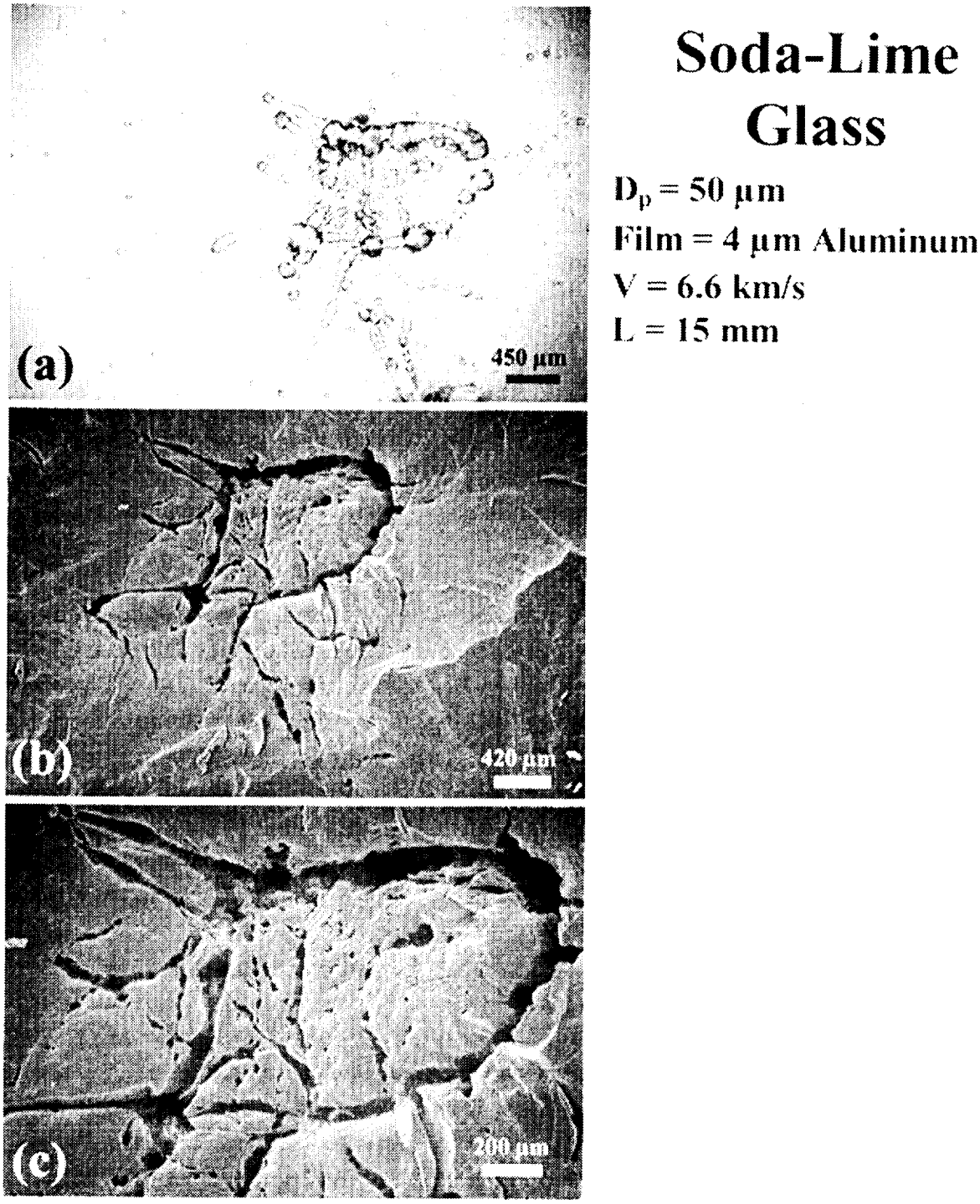

Figure 21a-c. (a) Optical and (b, c) SEM images of damage in 0.02-g/cm^3 aerogel by a severely fragmented and substantially molten projectile (see text).

In summarizing this section on aggregate particles of low-cohesive strength, we suggest that Figures 16-21 demonstrate successful production and hypervelocity impact of such particles. However, neither the mass nor actual encounter velocity can be documented with precision. As a result, these experiments remain highly qualitative. Nevertheless, they seem to demonstrate that such particle impacts are recognizable in aerogel targets. They produce compound penetration features characterized by stubby, bulbous penetration cavities from which any number of subsidiary, slender tracks of variable depth may emanate, the latter reflecting discrete, individual fragments. The presence of cocoa powder in some tracks and impactor residue at the termini suggest that natural aggregate particles of low bulk density and low-cohesive strength can be collected successfully with aerogel, at least at encounter velocities of up to 6 km/s.

7. Discussion

We have conducted a variety of experimental impacts into aerogels of variable density (0.01 to 0.05 g/cm^3), all of which were somewhat lower than the majority of previous studies (e.g., Barrett et al. [1992], Mendez [1995], Thomson [1995], and Burchell and Thomson [1996]). In addition, we conducted most of our experiments with projectiles (50 mm) that are smaller than those employed in past efforts (>100 mm, commonly >500 mm).

One of our major findings is an increased appreciation of the experimental difficulties that are involved when attempting to launch ensembles of small projectiles using a shotgun method. Most natural materials, which must be crushed for proper sizing, simply fail during the acceleration to typical light-gas gun velocities. It is not possible to grind coarse, raw stock without generating microcracks and other defects along which individual particles fail during launch. Nevertheless, a few intact particles might make it to the target in some cases. Unfortunately, the size, mass, and shape of any given particle will not be well-defined, because sieving operations are poorly suited to ensuring good reproducibility of these critical parameters, especially for particles <100 μm in diameter. These uncertainties in projectile properties necessitate considerable interpretative judgment on a track-by-track basis to differentiate between nominal impact events that are consistent with initial impact conditions and those that are not. Dedicated efforts are needed to reduce, and hopefully eliminate, the current uncertainties in projectile mass and shape for shot-gunned impactors of a few tens of microns in diameter.

With these reservations in mind, the calibration work presently available for aerogel targets is summarized in Figure 22, albeit on the basis of select data. Figure 22a includes only the deepest penetration tracks, either from the present experiments or as reported in the literature for specific impact conditions. The general agreement among a wide diversity of investigations, employing a wide variety of projectile materials, is noteworthy. There is a general trend of increasing track length with decreasing aerogel density, yet this trend is largely controlled by the present study. Note that the data illustrated in Figure 22a reflects a variety of particle velocities ranging from 5 to 7 km/s, and that there is no obvious trend regarding velocity dependence. Furthermore, all non-spherical materials that were crushed in the laboratory generated shorter penetration tracks than did the spherical impactors. This dichotomy possibly relates to modest yet efficient mass loss by increased chipping and rounding of irregular corners during light-gas gun launch and especially during early penetration of the aerogel targets.

Figure 22b presents a summary of existing work related to the maximum fraction of the initial projectile diameter preserved, either physically retrieved or measured in situ at the terminus of individual tracks. Again, these are high-graded data, depicting the *maximum* residue diameter (D_r), normalized to the nominal projectile diameter (D_p). As mentioned above, the spherical projectiles systematically yielded more residues than the crushed powders, with the latter barely amounting to 10% of the original mass in most cases. Once again, these data are difficult to interpret in an internally self-consistent manner.

On the basis of the preceding summary and in agreement with Thomson (1995) and Burchell and Thomson (1995), we conclude that the detailed penetration behavior of aerogel is presently poorly understood, as is the actual efficiency of particle capture. Current uncertainties result from poorly constrained experiments and will not improve until initial impact conditions are better defined. This is most readily accomplished by employing larger projectiles of more narrowly constrained mass and shape. This requires correspondingly larger and costlier aerogel targets and it has the additional disadvantage of moving the absolute scale of the experiments into a realm where its applicability to the capture of very small cosmic-dust particles, typically a few tens of microns in size, becomes questionable. Ideally, simulations with impactors much larger than those expected in space demands the use of aerogels of correspondingly dimensioned internal structures (e.g., Schmidt et al., 1994). None of these developments seems easy, and all would require dedicated efforts.

The experiments employing oblique impact angles confirm the results of Tsou (1990) and Thomson (1995) that the orientation of individual tracks faithfully records the angle of incidence and direction of projectile. In addition, the absolute track lengths observed in these experiments show that track length is *not* dependent on impact angle. This result alone suggests that high-velocity penetration of aerogel is unlike cratering in dense targets (e.g., Gault, 1973; Christiansen et al., 1993), but that it is strongly controlled by viscous drag and associated ablation as postulated by Anderson and Ahrens (1994). We do not understand the apparent weak dependence (if any) of track length on absolute impact velocity as suggested by the present data.

High-velocity impact of friable, low-density, porous particles into aerogel targets has been simulated at 5 to 7 km/s for the first time. One approach employed clods of fine-grained powder (cocoa), the other used collisionally generated clouds of glass fragments and melts. These experiments seem significant since a substantial fraction of cometary particles and interplanetary dust may be of low density and/or modest cohesion. The present experiments demonstrate that low-density, highly porous and fluffy aggregate particles form readily recognizable penetration tracks, and that residues do reside within such impact features, at least at experimental velocities around 6.5 km/s.

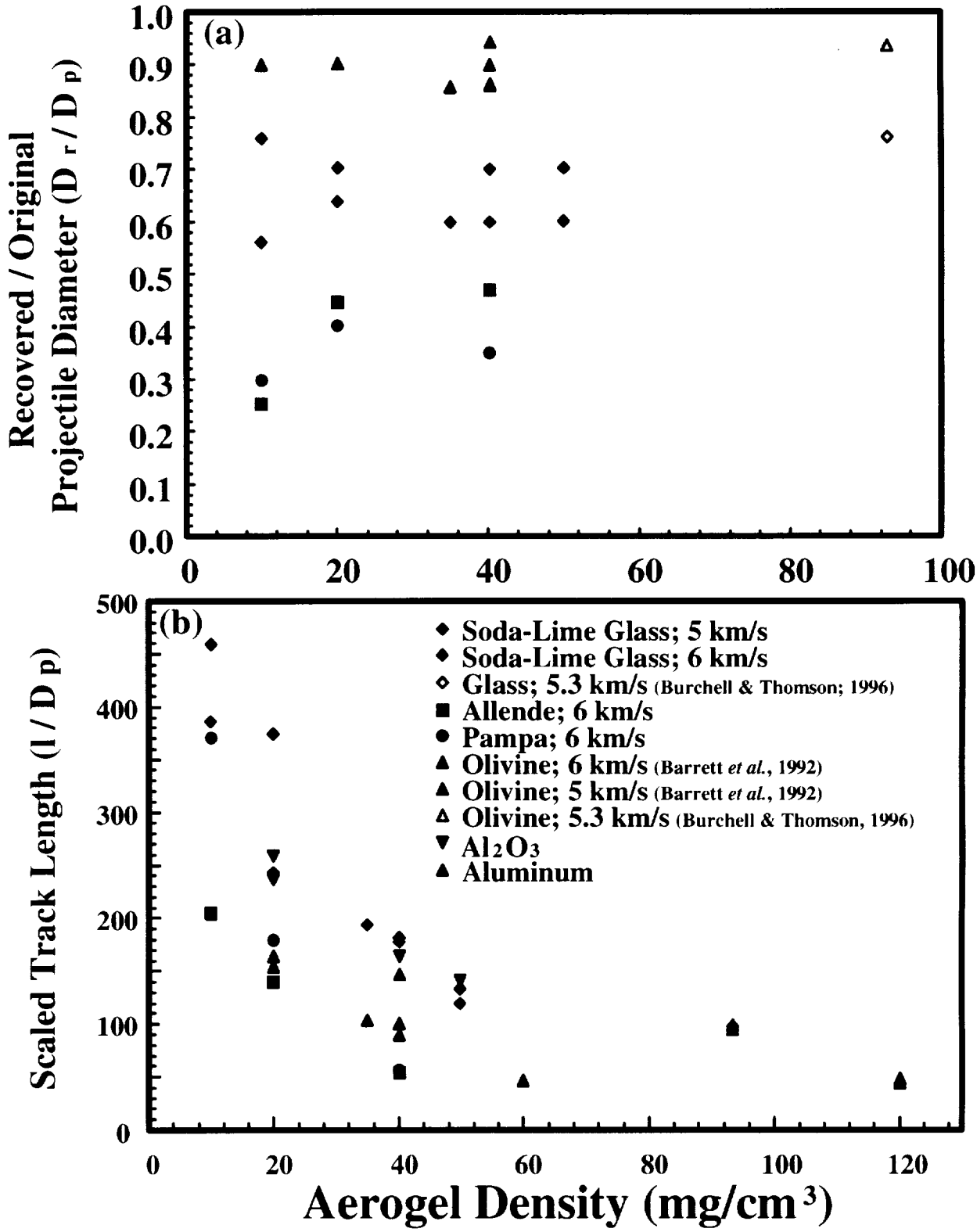

Figure 22. Summary of past and present experiments that employed projectiles smaller than 200 μm and aerogels of various densities. (a) Track length normalized to projectile diameter (l D_p) and (b) relative size of recovered residue (D_r D_p). Note that all data are high-graded and refer to either the longest tracks or largest residues for a given set of initial impact conditions. We ascribe most of the observed scatter in these figures to experimental difficulties in the form of either poorly characterized initial impactor size or poorly known aerogel density. Additional experiments are needed to try to resolve some of these ambiguities.

8. Conclusions

In support of ongoing flight instruments on board the *Mir* complex and of the Discovery Class *Stardust* sample return mission to Comet Wild 2, we have conducted a wide variety of impact experiments into aerogel targets. Most of these must be viewed as pilot-type tests to establish an improved understanding of the performance of low-density SiO_2-aerogel as a medium with which to trap hypervelocity particles. Aimed at providing high-fidelity tests of potential flight collectors, we experimented with unusually small projectiles (50 μm in diameter), and with aerogels of very low density (<0.05 g/cm^3), thereby complementing previous studies at typically larger projectile scales and higher aerogel densities. While we set out to relate initial impact conditions to the morphology of the observed penetration tracks and the mass of the recovered projectile, we encountered a number of experimental problems that prevented us from establishing the desired quantitative relationships.

Nevertheless, we fully concur with previous studies that aerogel is an excellent capture medium that will permit the collection of unmelted silicates at encounter velocities of 6 to 7 km/s. We were able to recover analyzable projectile residue from experiments with encounter velocities as high as 7 km/s, including metallic aluminum, aluminum oxide, powdered meteorites, powdered minerals, glass fragments, and even fine-grained powders. Consequently, we expect little difficulty differentiating between metallic and aluminum-oxide impactors among the particles trapped by the ODC collectors on board *Mir*, or in recovering cometary particles of a wide variety of physical and chemical properties via the upcoming *Stardust* mission.

However, on the basis of the current experiments, it could prove impractical to relate dimensional measurements of individual penetration tracks and associated projectile residues in space-exposed aerogels to detailed initial impact conditions, such as the original particle size, mass, and/or velocity. While improved impact simulations might provide more quantitative relationships than those presented here, it must be emphasized that a variety of concepts currently exist (e.g., Auer and Bun, 1994; Tuzzolino, 1994; and others) to determine these properties independently, including complete trajectory measurements on a particle-by-particle basis via "active" instruments. If required by scientific need, such active detectors can be readily combined with any passive aerogel collector.

Regardless, aerogel is a highly suitable, if not the most outstanding, capture medium over a wide range of initial impact conditions, including impact velocities as high as 7 km/s, possibly higher. Aerogel should not be faulted for yielding limited dynamic particle information. Its primary purpose and function is to trap the residue(s) of hypervelocity impactors, either natural or man-made. It does so extremely well and without peer.

9. References

Anderson, C.E., ed. (1993). Proc. Hypervel. Impact Symp. 1992, *Int. J. Impact Engin., 14, 1-4*, pp. 891.

Anderson, C.E., ed. (1995). Proc. Hypervel. Impact Symp. 1994, *Int. J. Impact Engin., 17, 1-6*, pp. 947.

Anderson, W., and Ahrens, T.J. (1994). Physics of interplanetary dust capture via impact into organic foam. *J. Geophys. Res. E* ***99***, pp. 2063-2071.

Auer, S. and Bun, O.V. (1994). Highly transparent and rugged sensor for velocity determinations of cosmic-dust particles. In *Workshop on Particle Capture, Recovery and Velocity/Trajectory Measurement Technologies* (M.E. Zolensky, ed.), Lunar and Planetary Institute, Houston, TX, *LPI Technical Report 94-05*, pp. 25-29.

Barrett, R.A.; Zolensky, M.E.; Hörz, F.; Lindstrom, D.; and Gibson, E.K. (1992). Suitability of SiO_2 aerogel as a capture medium for interplanetary dust. *Proc. 22nd Lunar Planet. Sci. Conf.*, pp. 203-212.

Bernhard, R.P.; Hörz, F.; and Kessler, D.J. (1996). Orbital debris impacts on the trailing edge of the Long-Duration Exposure Facility (LDEF). In *Proc. 1st International Workshop on Space Debris, Moscow*, 1995, to be published by Space Research Institute/National Academy of Sciences, Moscow (in press).

Brownlee, D.E.; Hörz, F.; Hrubesh, L.; McDonnell, J.A.M.; Tsou, P.; and Williams, J. (1994). Eureka! Aerogel capture of Meteoroids in space. *Lunar Planetary Sci. XXIV*, 183-184 (abstract).

Burchell, M.J. and Thomson, R. (1996). Intact hypervelocity capture in aerogel in the laboratory. In *Shock Compression of Condensed Matter-1995*, Schmidt, S.C. and Tao, W.C., eds., *AIP Conf. Proc. 370, Part 2*, pp. 1155-1158.

CDCF (1990), *Cosmic Dust Collection Facility: Scientific Objectives and Programmatic Relations*, CDCF Committee Report (F. Hörz, ed.), *NASA TM 102160*, p. 29.

Christiansen, E.L.; Cykowski, E.; and Ortega, J. (1993). Highly oblique impacts into thick and thin targets. *Int. J. Impact Engin.* ***14***, pp. 157-168.

Cintala, M. J. and Hörz, F. (1992). An experimental evaluation of mineral specific comminution, *Meteoritics 27*, pp. 395-403.

Fricke, L. (1988). Aerogels, *Scientific American* ***258***, pp. 92-97.

Gault, D.E. (1973). Displaced mass, depth, diameter, and effects of oblique trajectories for impact craters formed in dense, crystalline rocks. *The Moon 3*, pp. 32-44.

Grewing, M.; Praderie, F.; and Reinhard, R., eds. (1986). Exploration of Halley's Comet, Springer Verlag, Berlin, pp. 984.

Gwynn, D.W.; Hörz, F.; Bernhard, R.P.; and See, T.H. (1996). The dispersion of soda-lime glass projectiles following penetration of thin aluminum membranes. *Proc. HVIS 1996 Conf., Int. J. Impact Engin. Special Issue* (in print).

Hohler, V. and Stilp, A.V. (1987). Hypervelocity impact of rod projectiles from L/D from 1 to 32. *Int. J. Impact Engin.* **5**, pp. 323-332.

Hörz, F.; Cintala, M.J.; and Zolensky, M.E. (1992). Hypervelocity penetration tracks in very low-density, porous targets. In *Hypervelocity Impacts in Space* (J.A.M. McDonnell, ed.) Univ. of Kent at Canterbury, pp. 19-23.

Hörz, F.; Cintala, M.J.; Bernhard, R.P.; and See, T.H. (1994). Dimensionally scaled penetration experiments: Aluminum targets and glass projectiles 50 μm to 3.175 mm in diameter. *Int. J. Impact Engin.* ***15***, pp. 257-280.

Hrubesh, L.W. and Poco, J.F. (1990). Development of low-density silica aerogel as a capture medium for hypervelocity particles. *Lawrence Livermore National Laboratory Report UCLR-CR 105858 SUM,* p. 12.

Jessberger, E.K.; Rahe, J.; and Kissel, J. (1989). The Composition of Comets. In *Origin and Evolution of Planetary and Satellite Atmospheres* (Atreya, S.K.; Pollack, B.P.; and Matthews, M.S., eds.), The University of Arizona Press, Tucson, AZ, pp. 167-191.

Kissel J., et al. (1986). Composition of comet Halley dust particles from Giotto observations. *Nature* ***321***, pp. 280-282.

Love, S.G; Joswiak, D.J.; and Brownlee, D.E. (1993). Densities of 5-15 μm interplanetary dust particles, *Lunar Planet. Sci. XXIV,* 901-902 (abstract).

Maag, C. and Kelly-Linder, W. (1992). Results of Space Shuttle intact particle capture experiments. In *Hypervelocity Impacts in Space* (J.A.M. McDonnell, ed.), University of Canterbury, pp. 186-190.

Mendez, D.J. (1995). Physical Characterization of SiO_2 Aerogel: Phase I Final Report. *Lockheed Missiles and Space Co., Contractor Report LMSC-P0166*, pp. 95.

Orphal, D.L.; Anderson, C.E.; and Franzen, F.F. (1990). Impact calculations for L/D < 1 penetrators. *12th Int. Symp. on Ballistics*, San Antonio, TX.

Piekutowski, A. (1993). Characteristics of debris clouds produced by hypervelocity impact of aluminum spheres with thin aluminum plates. *Int. J. Impact. Engin.* ***14***, pp. 573-586.

Schmidt, R.M.; Housen, K.R.; Piekutowski, A.J.; and Poormon, K.L. (1994). Cadmium simulations of orbital debris shield performance to scaled velocities of 18 km/s *J. Spacecraft and Rockets* ***31***, pp. 866-877.

Thomson, R. (1995). An Investigation of the Intact Capture of Hypervelocity Particles in Aerogel. Unpublished MS Thesis, Univ. of Kent, Canterbury, UK, pp. 125.

Tsou, P. (1990). Intact capture of hypervelocity projectiles. *J. Int. Impact Engin.* ***10***, pp. 615-627.

Tsou, P. (1995). Silica aerogel captures cosmic dust intact. *J. Non-Crystalline Solids* ***186***, pp. 415-427.

Tsou, P.; Brownlee, D.E.; Lawrence, M.R.; Hrubesh, L.; and Albee, A.L. (1988). Intact capture of hypervelocity micrometeoroid analogues. *Lunar Planet. Conf. XIX,* 1205-1206 (abstract).

Tuzzolino, A.J. (1994). PVDF Flux/Mass/Velocity/Trajectory Systems and their applications in space. In *Workshop on Particle Capture, Recovery and Velocity/Trajectory Measurement Technologies,* Lunar and Planetary Institute, Houston, TX, *LPI Technical Report 94-05*, pp. 89-93.

Werle, V.; Fechtig, H.; and Schneider, E. (1981). Impact Accretion Experiments. *Proc. Lunar Planet. Sci. Conf. 12th*, pp. 1641-1647.

Zolensky, M.E., ed. (1994). *Workshop on Particle Capture, Recovery and Velocity/Trajectory Measurement Technologies*, Lunar and Planetary Institute, Houston, TX, *LPI Technical Report 94-05*, p. 102.

Zook, H.A. (1991). Deriving the velocity distribution of meteoroids from the measured meteoroid impact directionality on the various LDEF surfaces. In *LDEF - 69 Months in Space, First Post Retrieval Symposium,* A.S. Levine, ed., *NASA Conference Publication 3134*, pp. 569-581.

REPORT DOCUMENTATION PAGE

Form Approved
OMB No. 0704-0188

1. AGENCY USE ONLY *(Leave Blank)*	2. REPORT DATE	3. REPORT TYPE AND DATES COVERED
	April 1998	NASA Technical Memorandum

4. TITLE AND SUBTITLE
Capture of Hypervelocity Particles With Low-Density Aerogel

5. FUNDING NUMBERS

6. AUTHOR(S)
Friedrich Horz, Mark J. Cintala, Michael E. Zolensky, Ronald P. Bernhard*, William E. Davidson*, Gerald Haynes*, Thomas H. See*, Peter Tsou**, Donald E. Brownlee***

7. PERFORMING ORGANIZATION NAME(S) AND ADDRESS(ES)
Lyndon B. Johnson Space Center
Houston, Texas 77058

8. PERFORMING ORGANIZATION REPORT NUMBERS
S-838

9. SPONSORING/MONITORING AGENCY NAME(S) AND ADDRESS(ES)
National Aeronautics and Space Administration
Washington, D.C. 20546-0001

10. SPONSORING/MONITORING AGENCY REPORT NUMBER
TM-98-207192

11. SUPPLEMENTARY NOTES
* Lockheed-Martin Space Mission Systems and Services; ** Jet Propulsion Laboratory; ***Dept. of Astronomy/University of Washington

12a. DISTRIBUTION/AVAILABILITY STATEMENT
Unclassified/unlimited
Available from the NASA Center for AeroSpace Information (CASI)
800 Elkridge Landing Rd
Linthicum Heights, MD 21090-2934 (301) 621-0390 Subject Category: 88

12b. DISTRIBUTION CODE

13. ABSTRACT *(Maximum 200 words)*
Recent impact experiments conducted at Johnson Space Center supported a space-exposed flight instrument called the orbital debris collector (ODC) to see whether SiO2 aerogel performed adequately as a collector to capture cosmic dust particles and/or manmade debris, or whether additional development is needed. The first ODC was flown aboard the Mir for 18 months, while the second will be flown aboard a spacecraft (Stardust, to be launched in 1999) that will encounter the comet Wild 2 and return to Earth. Aerogels are highly porous materials that decelerate high-velocity particles without substantial melting or modifications to the particles' components; in other denser materials, these particles would melt or vaporize upon impact.

The experimental data in this report must be considered somewhat qualitative because they are characterized by substantial, if not intolerable, scatter, possibly due to experimental difficulties in duplicating given sets of initial impact conditions. Therefore, this report is a chronological guide of the experimenters' attempts, difficulties, progress, and evaluations for future tests.

14. SUBJECT TERMS	15. NUMBER OF PAGES	16. PRICE CODE
aerogel; space debris; cosmic dust; cometary atmospheres; deceleration; hypervelocity impact; impact melts	60	

17. SECURITY CLASSIFICATION OF REPORT	18. SECURITY CLASSIFICATION OF THIS PAGE	19. SECURITY CLASSIFICATION OF ABSTRACT	20. LIMITATION OF ABSTRACT
Unclassified	Unclassified	Unclassified	None